Syd/JIP3 Controls Tissue Size by Regulating Diap1 Protein Turnover Downstream of Yorkie/YAP

Vakil Ahmad, Gangadhar P. Vadla, Chiswili Y. Chabu

University of Missouri, Division of Biological Sciences,

Columbia, Missouri 65211

Corresponding author: C.Y. Chabu (chabuc@missouri.edu)

Highlights

- Syd/JIP3 is required for proper *Drosophila* wing size
- Syd/JIP3 stabilizes Diap1 to inhibit cell death in *Drosophila* and in mammalian cells
- Activation of Yorkie/YAP stimulates Syd/JIP3
- Yorkie-mediated tissue growth is highly sensitive to Syd/JIP3 dosage

Abstract

How organisms control organ size is not fully understood. We found that Syd/JIP3 is required for proper wing size in *Drosophila*. *JIP3* mutations are associated with organ size defects in mammals. The underlying mechanisms are not well understood. We discovered that Syd/JIP3 inhibition results in a downregulation of the inhibitor of apoptosis protein1 (Diap1) in the *Drosophila* wing. Correspondingly, Syd/JIP3 deficient tissues exhibit ectopic cell death and yield smaller wings. Syd/JIP3 inhibition generated similar effects in mammalian cells, indicating a conserved mechanism.

We found that Yorkie/YAP stimulates Syd/JIP3 in *Drosophila* and mammalian cells. Notably, Syd/JIP3 is required for the full effect of Yorkie-mediated tissue growth. Thus Syd/JIP3 regulation of Diap1 functions downstream of Yorkie/YAP to control growth.

This study provides mechanistic insights into the recent and perplexing link between *JIP3* mutations and organ size defects in mammals, including in humans where de novo *JIP3* variants are associated with microcephaly.

Introduction

The molecular basis of organ size regulation is a central question in developmental biology. Systemic signals such as insulin and growth factors play a key role in determining body and organ size. In *Drosophila*, starvation or genetic mutations in nutrient-sensing genes produce animals with smaller organs via well-defined and evolutionarily conserved mechanisms (Katsuyama et al., 2015; Stocker and Hafen, 2000). In addition to these systemic factors, transplantation experiments in salamander and in *Drosophila* have revealed that tissues possess intrinsic size control mechanisms. Salamander limbs maintain their size when transplanted onto animals with different limb sizes (Twitty V. C., 1931). Similarly, fragments of larval wing discs or young intact wings grow to reach normal size

48 when transplanted into the abdomen of adult flies (Bryant and Levinson, 1985). In contrast to
49 systemic signals, these tissue-intrinsic organ size control mechanisms are not well understood.
50 The *Drosophila* wing imaginal disc is a powerful experimental system to understand growth control
51 mechanisms. Embryonically derived cells undergo several rounds of cell proliferation to form a
52 mature epithelium that ultimately gives rise to an adult wing with stereotyped size and shape (Day
53 and Lawrence, 2000; Fristrom and Chihara, 1978; Garcia-Bellido, 1975; Garcia-Bellido and
54 Merriam, 1971; Mandaravally Madhavan and Schneiderman, 1977; Martin et al., 2009; Milan et al.,
55 1996; Worley et al., 2013). Genetic screens aimed at identifying mutations that deregulate growth in
56 this system have led to the discovery of key and broadly conserved tissue-intrinsic growth control
57 signaling pathways, including the Hippo pathway (reviewed in (Hariharan, 2015; Irvine and Harvey,
58 2015; Pan, 2007). In fly and mammalian tissues, Hippo signaling potently controls tissue size by
59 modulating the activity of Yorkie/YAP, a transcriptional co-activator for cell proliferation and cell
60 survival genes (Dong et al., 2007; Huang et al., 2005; Jia et al., 2003; Oh and Irvine, 2008; Pan,
61 2007). An earlier study reported that the c-Jun N-terminal kinase (JNK, also known as Bsk–FlyBase)
62 regulates Hippo in the developing wing to control wing size. Localized JNK activity represses Hippo
63 to allow Yorkie/YAP to drive cell proliferation throughout the tissue, hence promoting wing growth
64 (Willsey et al., 2016). The Hippo-Yorkie/YAP signal is a central tissue-size regulator, and its
65 function is well conserved across species. While research on Yorkie/YAP have generated significant
66 mechanistic insights into how Yorkie/YAP and its transcriptional program are regulated, much less
67 is known about developmental mechanisms for restraining Yorkie/YAP-mediated tissue growth to
68 achieve organ size stereotypy(Bernhard et al., 2000; Pan, 2007; Zheng and Pan, 2019).
69 Mitogen activating protein kinase (MAPK) scaffolding proteins mediate cellular responses to
70 apoptotic or proliferative signals. Sunday Driver (Syd) or JNK-interacting protein-3 (JIP3) belongs
71 to a family of conserved scaffolding proteins that bind to and facilitate JNK activation (Davis and

72 Tapon, 2019; Davis, 2000; Kelkar et al., 2000). Syd/JIP3 also regulates vesicle transport in worm
73 and mammalian cells (Caswell and Dickens, 2018; Choudhary et al., 2017; Edwards et al., 2013;
74 Gowrishankar et al., 2017; Sun et al., 2017; Taylor and Alessi, 2020).
75 Using the developing *Drosophila* wing as a model system, we found that Syd/JIP3 is required for
76 proper wing size. Mechanistic studies revealed that Syd/JIP3 functions downstream of Yorkie/YAP
77 by controlling the stability of Diap1, an important cell survival regulator and Yorkie/YAP target.
78 Syd/JIP3 regulates Diap1 post-transcriptionally by controlling its protein turnover. Congruent with
79 these observations, knocking down Syd/JIP3 has no effect on Diap1 transcription but leads to a loss
80 of Diap1 protein and correspondingly causes ectopic cell death, resulting in a smaller wing. Restoring
81 Diap1 protein in Syd/JIP3 knockdown tissues restores wing size. Importantly, activation of
82 Yorkie/YAP upregulates Syd/JIP3 protein and interfering with this stimulation suppresses
83 Yorkie/YAP-mediated tissue overgrowth. In addition to defining a novel growth control mechanism,
84 this work provides molecular insights into the perplexing association between *JIP3* mutations and
85 small brains in mice and humans (Kelkar et al., 2003; Platzer et al., 2019).
86

87 **Materials and Methods**

88 **Fly strains**

89 All the crosses were maintained at 25ºC unless otherwise described. Fly strains used for this study
90 are: *UAS-Syd-RNAi* (Bloomington Stock #43232), *UAS-Syd-RNAi* (VDRC Stock #35346), *UAS-*
91 *dSyd.GFP* (Mary K. Baylies), *Df(3L)syd*^{A2} (Bloomington Stock #32017), *syd*^{PL00426} (Bloomington
92 Stock #19495), *UAS-Bsk-DN* (Tian Xu), *UAS-Yki* (Doujia Pan), *UAS-Yki*$^{S111A.S168A.S250A}$
93 (Bloomington Stock #28817), *UAS-Hpo-RNAi* (Bloomington Stock #33614), *UAS-Diap1*
94 (Bloomington Stock #6657), *diap1-LacZ* (Bloomington Stock #12093), *diap1*$^{33\text{-}1s}$(Hermann Steller),
95 *fj-LacZ* (Bloomington Stock #44253), *CycE-lacZ* (Bloomington Stock #59065), *ex-lacZ*

96 (Bloomington Stock #44248), *Jub-GFP* (Bloomington Stock #56806), *dronc*^{51}(Bloomington Stock
97 #23284) including GAL4 drivers *Dcr2,engrailed-Gal4, nubbin-Gal4, patched-Gal4, hedgehog-Gal4*
98 *and gmr-Gal4.*

99 **Immunohistochemistry**

100 Wing imaginal discs were dissected, fixed, and stained as previously described (Chabu and Xu, 2014;
101 Pagliarini and Xu, 2003). The primary antibodies used were rabbit anti-PH3 (1:1000, Sigma); rabbit
102 anti-Diap1 (1:1000, Hermann Steller); rabbit anti-pWts (1:200, D. Pan), mouse anti-β-gal (1:1000,
103 Sigma). Secondary antibodies were from Invitrogen. Specimens were imaged on a Leica TCS SP8
104 confocal microscope. Images were analyzed and processed with IMARIS (Bitplane, Switzerland)
105 and illustrator software (Adobe).

106 **Western blots**

107 Wing imaginal discs from third-instar larvae were dissected and homogenized in lysis buffer (50 mM
108 HEPES pH 7.5, 150 mM KCl, 5 mM $MgCl_2$, 0.01% Triton-X) supplemented with protease and
109 phosphatase inhibitor cocktail (Cat #78443, Thermo Scientific). For cell culture, protein lysates were
110 prepared in lysis buffer (20 mM Tris-HCl pH-7.5, 150 mM NaCl, 1 mM Na2EDTA, 1 mM EGTA,
111 1% Triton, 2.5 mM sodium pyrophosphate, 1 mM β-glycerophosphate, 1 mM Na3VO4, 1 μg/ml
112 leupeptin) supplemented with protease and a phosphatase inhibitor cocktail (Cell Signaling #9803S).
113 Proteins were electrophoresed on SDS-PAGE using 4-15% Mini-PROTEAN® TGX™ precast gel
114 (Cat #456-1085, Bio-Rad), transferred onto Nitrocellulose membranes, and incubated with rabbit
115 anti-Diap1 (1:1000, Hermann Steller) or mouse anti-JIP3 (1:1000, Cat #46663, Santa Cruz), mouse
116 anti-HA (1:1000, Cat #7392, Santa Cruz), mouse anti-c-IAP(1:1000, Cat #271419, Santa Cruz),
117 rabbit anti-β-Actin (1:1000, Cat #4967, Cell Signaling Technology), mouse anti-GAPDH (0.3 μg/ml,
118 Cat #2G7, DSHB). Secondary antibodies used are anti-mouse horseradish peroxidase (HRP) (1:5000,

119 Cat #31430, Invitrogen) and anti-rabbit HRP (1:10000, Cat #31460, Invitrogen). Antibody signals
120 were detected using the ECL kit (Cat #32106, Thermo Fisher scientific) and ChemiDoc™ MP
121 Imaging System (Bio-Rad).

122 **Adult wing imaging and measurements**

123 Adult wings of female animals were dissected, mounted, flattened with glass slide, and imaged at
124 1.0X or 2.5X using Leica Microsystems, DMC 4500. In supplementary Figure 1, female flies were
125 washed with 75% ethanol and then with 95% ethanol for 2 min. Animals were dried on blotting paper
126 in oven at 50ºC for 2 min. Wings were removed and mounted on a glass slide in mineral oil, covered
127 with 22 × 40 mm coverslip and imaged at 2.5X. Areas of the adult wings were measured using the
128 *freehand selection* and *analyze* tools of ImageJ software 1.50i. P-values were calculated using the
129 two-tailed t-test function in Microsoft Excel.

130 **Cell death detection in *Drosophila***

131 For labeling dead cells with TUNEL assay, ApopTag® Red In Situ Apoptosis Detection Kit (Cat #
132 S7165) was used according to manufacturer's instruction. Briefly, dissected wing discs were fixed
133 and incubated in equilibration buffer at room temperature for 20 min followed by incubation with
134 terminal deoxynucleotidy transferase in reaction buffer for 1 h at 37ºC. Reaction was stopped using
135 stop buffer diluted in dH_2O. Disc were incubated with conjugated anti-digoxigenin antibodies for 2
136 h at room temperature, washed, and mounted using Vectashield mounting medium.

137
138 **Cell lines and cell culture**

139 Authenticated Human Embryonic Kidney 293 (HEK-293) cells were cultured in Dulbecco's
140 Modified Eagle Medium (#11965-092) supplemented with 10% FBS. TrypLE (Gibco#12604-021)
141 was used for immobilizing cells. Cells were counted in a Neubaur cell counter chamber following
142 Trypan Blue dead cell exclusion (Cat #T8154, Sigma). Dharmacon on-target siRNA-SMARTpool

143 plus Human scramble control (Cat #D-001810-10-05, Dharmacon) or JIP3 (Cat #L-003596-00-0005,
144 Dharmacon) were used for RNA interference experiments in HEK-293 cells. HEK 293 cells were
145 transfected with purified pCI-HA-YAP plasmid (Cat #27007, Addgene). DharmaFECT (Cat
146 #T2002-02, Dharmacon) was used for transfection. Protein knockdown was assessed 72 hours after
147 transfection.

148 **Real-time RT-PCR**

149 *Drosophila* wing tissues were dissected from 72-96 hours after egg-laying (AEL) or from 120-150
150 hours AEL wild-type animals for Syd/JIP3 quantitative real-time PCR (qRT-PCR). EZ Tissue/Cell
151 culture total RNA Miniprep kit (Cat #R1002-50, Bio Research) was used to extract RNA in
152 biological triplicates. The cDNA Reverse Transcription kit (Cat #4368814, Applied Biosystem) was
153 used to generate cDNA from 100 ng total RNA. SYBR Green iTaq Supermix (Bio-Rad) was used
154 for qRT-PCR. Expression of housekeeping gene *Rp49* (RpL32–FlyBase) was used as an internal
155 control. Primer sequences are as follows:

156 *Syd*: 5'-ACTTGACTCTACGCTGCGGCTGT-3' and 5'-GGTGCCGATCCACAGCCGGT-3'

157 *rp49*: 5′-GGCCCAAGATCGTGAAGAAG-3′ and 5′-ATTTG-TGCGACAGCTTAGCATATC-3′

158 **Flow cytometry analysis**

159 Flow cytometric detection of the cell death dye propidium iodide (PI) was used. PI was used at 10
160 μg/ml in PBS containing 1% BSA. PI was detected at 488/636 nm (excitation/emission) on an ADP
161 Beckman Coulter flow cytometer.

162 **Statistical analysis**

163 All *in vitro* experiments were reproducibly performed using biological triplicates. A student's *t-*
164 *test* was used for comparing the difference between two groups, and a $p < 0.05$ was considered as
165 statistically significant.

166

167 **Results**

168 We knocked down Syd/JIP3 in the developing wing (*nubGAL4>Syd-RNAi*) and this resulted in
169 smaller adult wings compared to controls (Figure 1A-E). A second Syd-RNAi line (v#35346)
170 similarly suppressed wing size (Supplemental Figure 1). Consistent with Syd/JIP3 inhibition, larval
171 wing tissues expressing either *Syd-RNAi* construct showed a reduction of Syd/JIP3 protein in
172 Western blot analyses. Anti-Syd/JIP3 Western blots detected two bands: a prominent ~147KD band
173 and a much weaker 135KD band in lysates derived from wild-type wing tissues. These bands were
174 considerably reduced in lysates obtained from wing tissues expressing *Syd-RNAi* (Figure 1F
175 Supplemental Figure 8A, C.). In addition, heterozygosity of two independent null alleles of *Syd*
176 (Bowman et al., 2000; Hacker et al., 2003) ($syd^{PL00426/A2}$) also yielded animals with smaller wings
177 compared to controls (Figure 2F, K). Taken together these data indicate that Syd/JIP3 regulates wing
178 size.

179 Interestingly, *JIP3* loss of function mutations are associated with brain size defects in mice and
180 humans (Kelkar et al., 2003; Platzer et al., 2019). We sought to determine the mechanism by which
181 Syd/JIP3 regulates tissue size.

182 The wing disc consists of a posterior (P) and an anterior (A) compartment. The patterning gene
183 *engrailed* is specifically expressed in the P compartment of the wing disc where it induces Hedgehog
184 (Hh) expression, while transcriptionally repressing Hh target genes (Garcia-Bellido, 1975; Tabata et
185 al., 1992; Zecca et al., 1995). Hh protein is transported via cell-to-cell exocytosis-endocytosis cycles
186 to the A compartment, where it activates Cubitus interuptus (Ci or Gli in vertebrates). In turn, Ci
187 stimulates the expression of dTRAF1 (*Drosophila* tumor necrosis factor receptor-associated factor-
188 1) a JNK pathway component, leading to JNK signaling activation at the P/A boundary. This
189 localized JNK activity acts via the LIM domain family protein Ajuba to repress Hippo signaling

190 throughout the entire tissue (Sun and Irvine, 2013; Willsey et al., 2016). It is unclear how this local
191 effect on Hippo signaling is transferred throughout the whole tissues to promote tissue growth.
192 We asked whether Syd/JIP3 regulates wing size via this Ci-JNK-Hippo signaling cascade. We turned
193 to *ptc-GAL4* to knockdown Syd/JIP3 in P/A boundary cells where JNK is normally active. We noted
194 that *ptc-GAL4* control wings were larger than their *nub-GAL4* counterpart controls (Figure 2A, K
195 versus Figure 1A, E). *ptcGAL4*-driven expression of *Syd-RNAi* generated wings that were smaller
196 than either parental control (*ptcGAL4 or Syd-RNAi*) wings (Figure 2G, K). These findings raised the
197 possibility that Syd/JIP3 regulates wing size via JNK.
198 To directly test this hypothesis, we performed genetic epistasis experiments between Syd/JIP3 and
199 JNK. We used the P/A boundary driver *ptcGAL4* to express a potent JNK inhibitor (dominant-
200 negative version of JNK, *Bsk-DN*) alone or in the presence of *Syd-RNAi* and determined the effect of
201 these manipulations on adult wing size. As expected, *Bsk-DN* reduced wing size compared to control
202 (Figure 2H, K). This size reduction effect was not as pronounced as what we had observed with *Syd-*
203 *RNAi* knockdown at the P/A boundary or throughout the wing tissue (*nubGAL4, Syd-RNAi*) (Figure
204 1A-E and Figure 2G, H, K). Importantly, blocking JNK failed to exacerbate the small wing
205 phenotype caused by Syd knockdown (*ptcGAL4>Bsk-DN, Syd-RNAi*). Instead, these wings
206 resembled Syd-depleted wings (Figure 2G-I, K). Moreover, overexpression of wild-type version of
207 *Syd* rescued the *Bsk-DN* small wing phenotype (Figure 2H, J, K). Collectively, these findings argue
208 that Syd/JIP3 is epistatic to JNK and that Syd/JIP3 functions downstream of JNK.
209 JNK acts via the LIM domain family protein Ajuba to repress Hippo signaling and promotes wing
210 growth (Willsey et al., 2016). Ajuba represses Hippo by sequestering Warts, a negative regulator of
211 Yorkie/YAP, to cell-cell junctions. This sequestration increases Yorkie/YAP activity, which
212 transcriptionally stimulates CyclinE and the E3-ubiquitin ligase *Drosophila* inhibitor of apoptosis
213 (Diap1) to simultaneously promote cell proliferation and inhibit cell death, hence promoting tissue

214 growth. How this Yorkie/YAP activation propagates throughout the whole tissue remains unclear.
215 Compared to wild-type controls, depleting Ajuba in the developing wing results in smaller adult
216 wings (Das Thakur et al., 2010; Marie et al., 2003; Rauskolb et al., 2014), similar to Syd knockdown.
217 We asked whether Syd is required for the junctional sequestration of Ajuba or Warts and found that
218 it is not. RNAi depletion of Syd in P/A boundary cells (*ptcGal4>Syd-RNAi*) did not reduce Ajuba
219 protein levels or alter its subcellular localization (Supplemental Figure 2A, B, *N*=22 discs).
220 Similarly, the subcellular localization of Warts in Syd knockdown cells was indistinguishable from
221 wild-type (Supplemental Figure 2A, C*, N=22* discs).
222 Next, we asked whether Syd/JIP3 acts downstream of Yorkie/YAP. *Patched is* expressed in a well-
223 defined 8-10 cells region along the P/A boundary. We used the *ptc-GAL4* promoter to co-express
224 *Yorkie* in this region. The *ptc-GAL4* line harbors a *UAS-GFP* construct in the background, making it
225 possible to quantitatively examine the effect of transgenes expression on tissue growth by scoring
226 the size of the GFP-positive tissue in confocal images. As expected, *ptc-GAL4* driven expression of
227 *Yorkie* resulted enlarged the P/A region compared to controls (Figure 3A, B, I) (Huang et al., 2005).
228 Co-expression of *Syd-RNAi* suppressed Yorkie-mediated tissue overgrowth (Figure 3B, C, I). The
229 suppressive effect of Syd knockdown on Yorkie-mediated tissue overgrowth is not specific to the
230 P/A domain. *Syd-RNAi* also suppressed Yorkie-mediated tissue overgrowth when Yorkie was over-
231 expressed in the posterior compartment or throughout the larval wing pouch (Supplemental Figure
232 3).
233 In a complementary approach, we activated Yorkie/YAP by repressing Hippo. In contrast to direct
234 Yorkie/YAP overexpression, this approach activates Yorkie/YAP at physiologically relevant levels.
235 We asked whether knocking down Syd in this context would also repress Yorkie/YAP-mediated
236 tissue overgrowth. As expected, Hippo knockdown resulted in larger wings compared to control
237 (Figure 3D, E, M). *Syd-RNAi* suppressed the large wing effect of Hippo inhibition (Figure 3E, F, H,

238 M). Moreover, heterozygosity of two independent *Syd* mutant alleles (*syd*$^{PL00426/+}$ or *syd*$^{A2/+}$) was
239 sufficient to significantly suppress *Hippo-RNAi* large wing phenotype (Figure 3E, G, M).
240 Collectively, the above findings suggested that Syd/JIP3 regulates wing size downstream or in
241 parallel to Yorkie/YAP. To distinguish between these possibilities, we asked whether Yorkie
242 activation stimulates Syd/JIP3 and it does. Western blot analyses showed that *Hippo-RNAi* triggers
243 the upregulation of Syd/JIP3 protein in *Drosophila* wing tissues (Figure 3J). In addition, expression
244 of Yorkie/YAP elevated Syd/JIP3 protein levels in *Drosophila* and mammalian (HEK293T) cells
245 (Figure 3K, L, and supplemental Figure 8C).
246 We sought to delineate the underlying mechanism. We examined the expression levels of two key
247 Hippo/Yorkie signaling transcriptional targets, Cyclin E (CycE) and Diap1 using standard
248 transcriptional reporter lines (CycE-LacZ and diap1-LacZ) (Jones et al., 2000; Zhang et al., 2008).
249 Interestingly, Diap1 and CycE expression levels were indistinguishable between wild-type and *Syd-*
250 *RNAi* expressing cells (Figure 4A, B and Supplemental Figure 4A-C). We extended these analyses
251 to include two additional Hippo signaling transcriptional targets *four-jointed* (fj) and *expanded* (Ex)
252 (Cho et al., 2006; Hamaratoglu et al., 2006) and found that Syd knockdown does not affect the
253 expression of *fj* or *Ex* (Supplemental Figure 4D-I). Thus, it is unlikely that Syd/JIP3 controls wing
254 size by regulating the Hippo transcriptional program.
255 We explored the possibility that Syd/JIP3 controls cellular response to Hippo signaling via a post-
256 translational mechanism and found that it does. Although RNAi knockdown of Syd in the posterior
257 compartment (*enGAL4, Syd-RNAi)* had no effect on Diap1 expression, immuno-staining experiments
258 using antibodies against Diap1 protein revealed a notable reduction of Diap1 protein levels (Figure
259 4A-D).
260 Due to constraints of some genetic manipulations and for practical reasons the posterior drivers *en-*
261 *GAL4* and *Hh-GAL4* are used interchangeably in the remaining experiments. We performed western

262 blot assays using lysates prepared from wild-type larval wing tissues or tissues expressing *Syd-RNAi*
263 in the posterior (*HhGAL4>Syd-RNAi*). Compared to wild-type controls, Syd knockdown in only half
264 of the cells was sufficient to show a reduction of Diap1 protein levels (Figure 4R). Diap1 normally
265 promotes cell survival by antagonizing the pro-apoptotic caspase Dronc (Nedd2-like caspase–
266 FlyBase) (Lee et al., 2011; Wilson et al., 2002). Concordant with a loss of Diap1 protein, Syd
267 knockdown in posterior compartment cells (*HhGAL4>Syd-RNAi*) resulted in ectopic cell death
268 compared to anterior compartment cells within the same tissues using TUNEL assays (Figure 4G,
269 H). Knocking down JIP3 in mammalian (HEK293) cells similarly suppressed the protein levels of c-
270 IAP (cellular inhibitor of apoptosis), increased cell death, and reduced cell numbers (Figure 4S-U).
271 These findings argue that Syd/JIP3 controls Diap1 turnover and that this mechanism is conserved.
272 The E3 ubiquitin ligase function of the Diap1 RING finger domain enables Diap1 to degrade not
273 only downstream substrates, but also itself to modulate cell survival (Ryoo et al., 2002; Yoo, 2005;
274 Yoo et al., 2002). Similar to inhibitor of apoptosis (IAP) proteins in vertebrates, Diap1 dimerizes and
275 self-ubiquitinates via its RING domain to trigger its own proteolysis (Feltham et al., 2011; Mace et
276 al., 2008; Rumpf et al., 2011; Silke et al., 2005). Ectopic expression experiments have shown that
277 inhibition of the RING domain via point mutations or deletions (RINGΔ) results in a significant
278 stabilization of not only the mutant protein but also endogenous wild-type Diap1, consistent with
279 Diap1 dimerization (Wilson et al., 2002; Yokokura et al., 2004). RING domain defective *diap1*
280 mutants are homozygous lethal but heterozygous viable, presumably because RINGΔ–wild-type
281 Diap1 heterodimers still retain some ability to inhibit Dronc and promote cell survival (Lisi et al.,
282 2000; Wilson et al., 2002; Yokokura et al., 2004). We asked to what extent diap1 RINGΔ
283 heterozygosity restores Diap1 protein levels in Syd/JIP3 knocked down cells.
284 We took advantage of a heterozygous viable *diap1* RINGΔ mutation [$diap1^{(33\text{-}1s)}$] (Wilson et al.,
285 2002) and asked whether its heterozygosity rescues Diap1 in Syd/JIP3-depleted wings.

286 Heterozygosity of the *diap1*$^{(33\text{-}1s)}$ allele [*diap1*$^{(33\text{-}1s)/+}$] restored Diap1 protein levels in *Syd-RNAi*
287 expressing cells (*enGAL4>Syd-RNAi, diap1*$^{(33\text{-}1)s/+}$, Figure 4C-F; 71%, *N=14*) and correspondingly
288 rescued wing size (Figure 4I-M, O, Q). Thus, Syd/JIP3 controls tissues size via Diap1.
289 Also, given the loss of Diap1 protein in Syd/JIP3-depleted tissues and the resulting ectopic cell death,
290 this would elevate Dronc activity. We predicted that Syd/JIP3-depleted tissues would be sensitive to
291 Dronc dosage such that a partial reduction of Dronc function (Dronc haploinsufficiency, *dronc*$^{51/+}$)
292 will be sufficient to restore wing size to some extents. Indeed, heterozygosity of a *dronc* null allele
293 (*dronc*^{51}) rescued wing size in *Syd-RNAi* animals (Figure 4I, K, L, N, P, Q).
294 Finally, we turned to HEK-293 cells to assess whether Syd/JIP3 similarly regulates cell survival and
295 cell growth in mammalian cells. RNAi knockdown of JIP3 inhibited the growth of HEK-293 cells
296 and caused ectopic cell death in flow cytometric assays (Figure 4S-U), mimicking Syd/JIP3
297 knockdown in *Drosophila*. Collectively, these findings highlight a novel and conserved Syd/JIP3
298 growth control mechanism. Our data indicate that Syd/JIP3 controls tissue size downstream of the
299 Yorkie/YAP by regulating Diap1 protein turnover, hence modulating cell survival and ultimately
300 tissue size.
301
302 **Discussion**
303 Our understanding of the molecular underpinnings of organ size regulation is incomplete. Genetic
304 screens in *Drosophila* imaginal discs have led to the identification of Hippo signaling as a central
305 and evolutionarily conserved growth control mechanism. More recently Willsey and colleagues
306 reported that in *Drosophila*, developmentally encoded signals trigger JNK activation at the posterior-
307 anterior boundary of the developing wing. This localized JNK activity, broadly inhibits Hippo
308 signaling to promote tissue-wide cell proliferation, resulting in a properly sized adult wing (Willsey

309 et al., 2016). Here we show that Syd/JIP3 regulates wing size downstream of Yorkie by controlling
310 Diap1 protein turnover.
311 Direct activation of Yorkie/YAP potently triggers tissue overgrowth in vertebrates and *Drosophila*.
312 Syd knockdown partly suppresses Yorkie/YAP-mediated tissue overgrowth. The moderate effect is
313 likely because direct activation of Yorkie/YAP is so potent that the resulting ectopic cell proliferation
314 masks the impact of *Syd-RNAi/Diap1*-mediated cell death in these tissues. Consistent with this,
315 depletion of Syd protein under three independent experimental conditions (*Syd-RNAi* or Syd
316 haploinsufficiency using $Syd^{PL00426}$ or Syd^{A2} loss of function alleles) suppressed the large wing
317 phenotype caused by a more moderate Yorkie activation (Hippo knockdown).
318 Activation of Yorkie/YAP either via Hippo knockdown or direct Yorkie/YAP overexpression
319 resulted in the upregulation of Syd/JIP3 protein in Drosophila and mammalian cells. These findings
320 are consistent with Syd/JIP3 acting downstream of Yorkie/YAP signaling.
321 Syd/JIP3 regulates growth by controlling Diap1 protein stability. Inhibition of Syd/JIP3 decreases
322 Diap1 protein levels and correspondingly triggers ectopic cell death in *Drosophila* and in mammalian
323 cells. Similar to *Syd-RNAi*, expression of *Diap1-RNAi* in P/A cells is sufficient to reduce adult wing
324 size (Supplemental Figure 6). Partial restoration of Diap1 rescues the small wing effect of Syd/JIP3
325 inhibition. The partial rescue may reflect an incomplete restoration of Diap1 protein and/or that the
326 re-established pool of Diap1 is only partly effective at inhibiting cell death. We cannot rule out the
327 possibility that Syd/JIP3 tissue size regulation involves additional Diap1-independent mechanisms.
328 The observation that Diap1 RINGΔ heterozygosity restores Diap1 protein levels in Syd/JIP3
329 knockdown cells supports the notion that Syd/JIP3 normally stabilizes Diap1 by protecting it from
330 proteolytic degradation.

331 Ectopic cell death is the primary mechanism underlying the reduced growth of Syd knockdown
332 *Drosophila* tissues and human cells. We did not detect a decrease of proliferative capacity in *Syd-*
333 *RNAi* expressing *Drosophila* tissues compared to wild-type controls (Supplemental Figure 5).
334 This study has identified Syd/JIP3 as a novel size regulator downstream of Hippo. It is tempting to
335 speculate that Syd/JIP3 regulation of Diap1 likely represents a robustness mechanism for Yorkie-
336 mediated tissue growth. *Syd/JIP3* is expressed at higher levels during the rapid growth phase (72-
337 96 hours after egg laying-AEL) and progressively drops later (120-150 hours AEL) when growth
338 slows down (Supplemental Figure 7). High Syd/JIP3 levels would stabilize Yorkie-activated Diap1,
339 permitting sustained tissue growth phase. The decline of Syd/JIP3 transcription later in development
340 would target Diap1 for degradation, thereby allowing cell death to sporadically occur throughout the
341 tissue, hence scaling down tissue response to Yorkie and contributing to size stereotypy.
342 Additional significance can be derived from the fact that our findings provide potential mechanistic
343 insights into the recent and perplexing link between *JIP3* mutations and organ size defects in
344 mammals, including humans where de novo *JIP3* variants are associated with microcephaly (Kelkar
345 et al., 2003; Platzer et al., 2019).
346

347 **Acknowledgment**

348 We thank A. Bergmann, G Halder, T. Xu, H. Steller, M. Baylies and D. Pan for antibodies and fly
349 stocks. We also thank BDSC and VDRC for fly lines. We also thank M. Kroll for comments on the
350 manuscript.
351

352 **Reference**

353 Bernhard, E.J., Stanbridge, E.J., Gupta, S., Gupta, A.K., Soto, D., Bakanauskas, V.J., Cerniglia,
354 G.J., Muschel, R.J., McKenna, W.G., 2000. Direct evidence for the contribution of activated N-ras
355 and K-ras oncogenes to increased intrinsic radiation resistance in human tumor cell lines. Cancer
356 Res 60, 6597-6600.

357 Bowman, A.B., Kamal, A., Ritchings, B.W., Philp, A.V., McGrail, M., Gindhart, J.G., Goldstein,
358 L.S., 2000. Kinesin-dependent axonal transport is mediated by the sunday driver (SYD) protein.
359 Cell 103, 583-594.
360 Bryant, P.J., Levinson, P., 1985. Intrinsic growth control in the imaginal primordia of Drosophila,
361 and the autonomous action of a lethal mutation causing overgrowth. Dev Biol 107, 355-363.
362 Caswell, P.T., Dickens, M., 2018. JIP3 localises to exocytic vesicles and focal adhesions in the
363 growth cones of differentiated PC12 cells. Mol Cell Biochem 444, 1-13.
364 Chabu, C., Xu, T., 2014. Oncogenic Ras stimulates Eiger/TNF exocytosis to promote growth.
365 Development 141, 4729-4739.
366 Cho, E., Feng, Y., Rauskolb, C., Maitra, S., Fehon, R., Irvine, K.D., 2006. Delineation of a Fat
367 tumor suppressor pathway. Nat Genet 38, 1142-1150.
368 Choudhary, B., Kamak, M., Ratnakaran, N., Kumar, J., Awasthi, A., Li, C., Nguyen, K.,
369 Matsumoto, K., Hisamoto, N., Koushika, S.P., 2017. UNC-16/JIP3 regulates early events in
370 synaptic vesicle protein trafficking via LRK-1/LRRK2 and AP complexes. PLoS Genet 13,
371 e1007100.
372 Das Thakur, M., Feng, Y., Jagannathan, R., Seppa, M.J., Skeath, J.B., Longmore, G.D., 2010.
373 Ajuba LIM proteins are negative regulators of the Hippo signaling pathway. Curr Biol 20, 657-662.
374 Davis, J.R., Tapon, N., 2019. Hippo signalling during development. Development 146.
375 Davis, R.J., 2000. Signal transduction by the JNK group of MAP kinases. Cell 103, 239-252.
376 Day, S.J., Lawrence, P.A., 2000. Measuring dimensions: the regulation of size and shape.
377 Development 127, 2977-2987.
378 Dong, J., Feldmann, G., Huang, J., Wu, S., Zhang, N., Comerford, S.A., Gayyed, M.F., Anders,
379 R.A., Maitra, A., Pan, D., 2007. Elucidation of a universal size-control mechanism in Drosophila
380 and mammals. Cell 130, 1120-1133.
381 Edwards, S.L., Yu, S.C., Hoover, C.M., Phillips, B.C., Richmond, J.E., Miller, K.G., 2013. An
382 organelle gatekeeper function for Caenorhabditis elegans UNC-16 (JIP3) at the axon initial
383 segment. Genetics 194, 143-161.
384 Feltham, R., Bettjeman, B., Budhidarmo, R., Mace, P.D., Shirley, S., Condon, S.M., Chunduru,
385 S.K., McKinlay, M.A., Vaux, D.L., Silke, J., Day, C.L., 2011. Smac mimetics activate the E3
386 ligase activity of cIAP1 protein by promoting RING domain dimerization. J Biol Chem 286,
387 17015-17028.
388 Fristrom, D., Chihara, C., 1978. The mechanism of evagination of imaginal discs of Drosophila
389 melanogaster. V. Evagination of disc fragments. Dev Biol 66, 564-570.
390 Garcia-Bellido, A., 1975. Genetic control of wing disc development in Drosophila. Ciba Found
391 Symp 0, 161-182.
392 Garcia-Bellido, A., Merriam, J.R., 1971. Parameters of the wing imaginal disc development of
393 Drosophila melanogaster. Dev Biol 24, 61-87.
394 Gowrishankar, S., Wu, Y., Ferguson, S.M., 2017. Impaired JIP3-dependent axonal lysosome
395 transport promotes amyloid plaque pathology. J Cell Biol 216, 3291-3305.
396 Hacker, U., Nystedt, S., Barmchi, M.P., Horn, C., Wimmer, E.A., 2003. piggyBac-based
397 insertional mutagenesis in the presence of stably integrated P elements in Drosophila. Proc Natl
398 Acad Sci U S A 100, 7720-7725.
399 Hamaratoglu, F., Willecke, M., Kango-Singh, M., Nolo, R., Hyun, E., Tao, C., Jafar-Nejad, H.,
400 Halder, G., 2006. The tumour-suppressor genes NF2/Merlin and Expanded act through Hippo
401 signalling to regulate cell proliferation and apoptosis. Nat Cell Biol 8, 27-36.
402 Hariharan, I.K., 2015. Organ Size Control: Lessons from Drosophila. Dev Cell 34, 255-265.

403 Huang, J., Wu, S., Barrera, J., Matthews, K., Pan, D., 2005. The Hippo signaling pathway
404 coordinately regulates cell proliferation and apoptosis by inactivating Yorkie, the Drosophila
405 Homolog of YAP. Cell 122, 421-434.
406 Irvine, K.D., Harvey, K.F., 2015. Control of organ growth by patterning and hippo signaling in
407 Drosophila. Cold Spring Harb Perspect Biol 7.
408 Jia, J., Zhang, W., Wang, B., Trinko, R., Jiang, J., 2003. The Drosophila Ste20 family kinase
409 dMST functions as a tumor suppressor by restricting cell proliferation and promoting apoptosis.
410 Genes & development 17, 2514-2519.
411 Jones, L., Richardson, H., Saint, R., 2000. Tissue-specific regulation of cyclin E transcription
412 during Drosophila melanogaster embryogenesis. Development 127, 4619-4630.
413 Katsuyama, T., Comoglio, F., Seimiya, M., Cabuy, E., Paro, R., 2015. During Drosophila disc
414 regeneration, JAK/STAT coordinates cell proliferation with Dilp8-mediated developmental delay.
415 Proc Natl Acad Sci U S A 112, E2327-2336.
416 Kelkar, N., Delmotte, M.H., Weston, C.R., Barrett, T., Sheppard, B.J., Flavell, R.A., Davis, R.J.,
417 2003. Morphogenesis of the telencephalic commissure requires scaffold protein JNK-interacting
418 protein 3 (JIP3). Proc Natl Acad Sci U S A 100, 9843-9848.
419 Kelkar, N., Gupta, S., Dickens, M., Davis, R.J., 2000. Interaction of a mitogen-activated protein
420 kinase signaling module with the neuronal protein JIP3. Mol Cell Biol 20, 1030-1043.
421 Lee, T.V., Fan, Y., Wang, S., Srivastava, M., Broemer, M., Meier, P., Bergmann, A., 2011.
422 Drosophila IAP1-mediated ubiquitylation controls activation of the initiator caspase DRONC
423 independent of protein degradation. PLoS Genet 7, e1002261.
424 Lisi, S., Mazzon, I., White, K., 2000. Diverse domains of THREAD/DIAP1 are required to inhibit
425 apoptosis induced by REAPER and HID in Drosophila. Genetics 154, 669-678.
426 Mace, P.D., Linke, K., Feltham, R., Schumacher, F.R., Smith, C.A., Vaux, D.L., Silke, J., Day,
427 C.L., 2008. Structures of the cIAP2 RING domain reveal conformational changes associated with
428 ubiquitin-conjugating enzyme (E2) recruitment. J Biol Chem 283, 31633-31640.
429 Mandaravally Madhavan, M., Schneiderman, H.A., 1977. Histological analysis of the dynamics of
430 growth of imaginal discs and histoblast nests during the larval development ofDrosophila
431 melanogaster. Wilehm Roux Arch Dev Biol 183, 269-305.
432 Marie, H., Pratt, S.J., Betson, M., Epple, H., Kittler, J.T., Meek, L., Moss, S.J., Troyanovsky, S.,
433 Attwell, D., Longmore, G.D., Braga, V.M., 2003. The LIM protein Ajuba is recruited to cadherin-
434 dependent cell junctions through an association with alpha-catenin. J Biol Chem 278, 1220-1228.
435 Martin, F.A., Herrera, S.C., Morata, G., 2009. Cell competition, growth and size control in the
436 Drosophila wing imaginal disc. Development 136, 3747-3756.
437 Milan, M., Campuzano, S., Garcia-Bellido, A., 1996. Cell cycling and patterned cell proliferation
438 in the wing primordium of Drosophila. Proc Natl Acad Sci U S A 93, 640-645.
439 Oh, H., Irvine, K.D., 2008. In vivo regulation of Yorkie phosphorylation and localization.
440 Development 135, 1081-1088.
441 Pagliarini, R.A., Xu, T., 2003. A genetic screen in Drosophila for metastatic behavior. Science 302,
442 1227-1231.
443 Pan, D., 2007. Hippo signaling in organ size control. Genes Dev 21, 886-897.
444 Platzer, K., Sticht, H., Edwards, S.L., Allen, W., Angione, K.M., Bonati, M.T., Brasington, C.,
445 Cho, M.T., Demmer, L.A., Falik-Zaccai, T., Gamble, C.N., Hellenbroich, Y., Iascone, M., Kok, F.,
446 Mahida, S., Mandel, H., Marquardt, T., McWalter, K., Panis, B., Pepler, A., Pinz, H., Ramos, L.,
447 Shinde, D.N., Smith-Hicks, C., Stegmann, A.P.A., Stobe, P., Stumpel, C., Wilson, C., Lemke, J.R.,
448 Di Donato, N., Miller, K.G., Jamra, R., 2019. De Novo Variants in MAPK8IP3 Cause Intellectual
449 Disability with Variable Brain Anomalies. Am J Hum Genet 104, 203-212.

450 Rauskolb, C., Sun, S., Sun, G., Pan, Y., Irvine, K.D., 2014. Cytoskeletal tension inhibits Hippo
451 signaling through an Ajuba-Warts complex. Cell 158, 143-156.
452 Rumpf, S., Lee, S.B., Jan, L.Y., Jan, Y.N., 2011. Neuronal remodeling and apoptosis require VCP-
453 dependent degradation of the apoptosis inhibitor DIAP1. Development 138, 1153-1160.
454 Ryoo, H.D., Bergmann, A., Gonen, H., Ciechanover, A., Steller, H., 2002. Regulation of
455 Drosophila IAP1 degradation and apoptosis by reaper and ubcD1. Nat Cell Biol 4, 432-438.
456 Sabino, D., Brown, N.H., Basto, R., 2011. Drosophila Ajuba is not an Aurora-A activator but is
457 required to maintain Aurora-A at the centrosome. J Cell Sci 124, 1156-1166.
458 Silke, J., Kratina, T., Chu, D., Ekert, P.G., Day, C.L., Pakusch, M., Huang, D.C., Vaux, D.L., 2005.
459 Determination of cell survival by RING-mediated regulation of inhibitor of apoptosis (IAP) protein
460 abundance. Proc Natl Acad Sci U S A 102, 16182-16187.
461 Stocker, H., Hafen, E., 2000. Genetic control of cell size. Curr Opin Genet Dev 10, 529-535.
462 Sun, G., Irvine, K.D., 2013. Ajuba family proteins link JNK to Hippo signaling. Sci Signal 6, ra81.
463 Sun, T., Li, Y., Li, T., Ma, H., Guo, Y., Jiang, X., Hou, M., Huang, S., Chen, Z., 2017. JIP1 and
464 JIP3 cooperate to mediate TrkB anterograde axonal transport by activating kinesin-1. Cell Mol Life
465 Sci 74, 4027-4044.
466 Tabata, T., Eaton, S., Kornberg, T.B., 1992. The Drosophila hedgehog gene is expressed
467 specifically in posterior compartment cells and is a target of engrailed regulation. Genes Dev 6,
468 2635-2645.
469 Taylor, M., Alessi, D.R., 2020. Advances in elucidating the function of leucine-rich repeat protein
470 kinase-2 in normal cells and Parkinson's disease. Curr Opin Cell Biol 63, 102-113.
471 Twitty V. C., S.J.L., 1931. The growth of eyes and limbs transplanted heteroplastically between
472 two species of Amblystoma. J. Exp. Zool. 59, 61-86.
473 Willsey, H.R., Zheng, X., Carlos Pastor-Pareja, J., Willsey, A.J., Beachy, P.A., Xu, T., 2016.
474 Localized JNK signaling regulates organ size during development. Elife 5.
475 Wilson, R., Goyal, L., Ditzel, M., Zachariou, A., Baker, D.A., Agapite, J., Steller, H., Meier, P.,
476 2002. The DIAP1 RING finger mediates ubiquitination of Dronc and is indispensable for
477 regulating apoptosis. Nat Cell Biol 4, 445-450.
478 Worley, M.I., Setiawan, L., Hariharan, I.K., 2013. TIE-DYE: a combinatorial marking system to
479 visualize and genetically manipulate clones during development in Drosophila melanogaster.
480 Development 140, 3275-3284.
481 Yokokura, T., Dresnek, D., Huseinovic, N., Lisi, S., Abdelwahid, E., Bangs, P., White, K., 2004.
482 Dissection of DIAP1 functional domains via a mutant replacement strategy. J Biol Chem 279,
483 52603-52612.
484 Yoo, S.J., 2005. Grim stimulates Diap1 poly-ubiquitination by binding to UbcD1. Mol Cells 20,
485 446-451.
486 Yoo, S.J., Huh, J.R., Muro, I., Yu, H., Wang, L., Wang, S.L., Feldman, R.M., Clem, R.J., Muller,
487 H.A., Hay, B.A., 2002. Hid, Rpr and Grim negatively regulate DIAP1 levels through distinct
488 mechanisms. Nat Cell Biol 4, 416-424.
489 Zecca, M., Basler, K., Struhl, G., 1995. Sequential organizing activities of engrailed, hedgehog and
490 decapentaplegic in the Drosophila wing. Development 121, 2265-2278.
491 Zhang, L., Ren, F., Zhang, Q., Chen, Y., Wang, B., Jiang, J., 2008. The TEAD/TEF family of
492 transcription factor Scalloped mediates Hippo signaling in organ size control. Developmental cell
493 14, 377-387.
494 Zheng, Y., Pan, D., 2019. The Hippo Signaling Pathway in Development and Disease.
495 Developmental cell 50, 264-282.
496

497

498 **Competing interests**

499 None

500 **Author Contributions**

501 V.A and C.Y.C designed the research. V.A performed *Drosophila* experiments and analyzed the

502 data together with C.Y.C. G.P.V performed tissue culture experiments. C.Y.C wrote the

503 manuscript.

504 **Figure Legends**

505 **Figure 1. Syd/JIP3 regulates adult wing size**

506 (A-D) Representative images showing adult wings from female animals of the indicated genotypes.

507 Wings from *nubGAL4* or *Syd-RNAi* parental lines are shown in (A) and (B), respectively. (C) Image

508 showing the effect of Syd knockdown (*nubGAL4*, *Syd-RNAi*). (D) Image of a pseudo-color overlay

509 of (A) (shown in brown) and (C) (shown in light indigo). (E) Quantification of wing size. For this

510 and all subsequent quantification figures, plotted values indicate the mean ±SD. The number of

511 tissues analyzed (N) per genotype is indicated inside the bar. All experiments were repeated at least

512 twice. *P*-value is computed from a t-test: p-value < 10^{-20} = ******, p-value = 10^{-20}– 10^{-10} = *****,

513 p-value = 10^{-10} –10^{-5} = ****, p-value = 10^{-5} – 10^{-3} = ***, p-value=10^{-3} – 10^{-2} = **, p-value = 0.01 –

514 0.05 = *, p-value ≥ 0.05 = not significant, ns. (F) Western blot image showing Syd/JIP3 protein

515 abundance in third-instar wing disc lysates derived from animals expressing *RFP* alone (control) or

516 co-expressing *Syd-RNAi* in the whole disc proper using *nubGAL4*. Blots were stained with anti-

517 Syd/JIP3 or GAPDH (loading control) antibodies.

518 **Figure 2. Syd/JIP3 functions downstream of JNK**

519 (A-J) Representative images showing adult wings from female animals of the indicated genotypes.
520 Wing images from control parental fly lines are shown in (A-E). (F-J) Pseudo-color overlay of wing
521 images dissected from *ptcGAL4* control (brown) or from $Syd^{PL00426}/Syd^{A2}$ trans-heterozygote animals
522 (indigo) (F) or animals expressing *Syd-RNAi* (G) or *Bsk-DN* (H) or co-expressing *Syd-RNAi* and *Bsk-*
523 *DN* (I) or wild-type *Syd* and *Bsk-DN* (J) all under the control of *ptcGAL4*. (K) Quantification of (A-
524 J).

525 **Figure 3. Syd/JIP3 functions in the Hippo pathway**

526 (A-C) Images of wing imaginal discs from age-controlled animals expressing *GFP* alone (A) or co-
527 expressing *Yorkie* (B) or co-expressing *Yorkie* and *Syd-RNAi* (C) under the control of *ptc-GAL4*.
528 Under wild-type condition *ptc-GAL4* expresses GFP in 8-10 cells along the posterior-anterior
529 boundary (A). Overexpression of Yorkie causes expands the size of the GFP-positive region (B). Syd
530 knockdown in Yorkie reduces the Yorkie-mediated tissue overgowth (C). The dotted lines denote
531 the posterior-anterior domain where transgenes were introduced. Size quantification of the GFP-
532 positive tissue across experimental conditions using confocal images and the image data analysis
533 platform IMARIS@BITPLANE data(E). (D-H) Representative images showing adult wings from
534 female animals of the indicated genotypes. Compared to *nubGAL4* control wings (D), expression of
535 *Hippo-RNAi* increases wing size (E). *Syd* haploinsufficiency ($Syd^{PL00426/+}$) suppresses the size effect
536 of *Hippo-RNAi* expression (F). Pseudo-color overlay wing images are shown in (G and H). (G) Wings
537 expressing *Hippo-RNAi* in the absence or presence of Syd haploinsufficiency ($Syd^{PL00426/+}$) are shown
538 in brown and indigo, respectively. (H) Wings expressing *Hippo-RNAi* in the absence or presence of
539 *Syd-RNAi* are shown in brown and indigo, respectively. (I) Quantification of relative volume of *GFP*-
540 positive tissue in A-C. (J) Western blot image showing Syd/JIP3 protein abundance in dissected wing
541 disc lysates from control (*nub-GAL4*) or Hippo-depleted (*nubGAL4>Hpo-RNAi*) tissues. Blots were

542 stained with anti-Syd/JIP3 or anti β-actin (loading control). (K) Western blot image showing
543 Syd/JIP3 protein abundance in dissected wing disc lysates from control tissues (*nub-GAL4*) or
544 tissues over-expressing Yorkie (*nubGAL4>Yorkie*) tissues. Blots were stained with anti-Syd/Jip3 or
545 GAPDH antibodies (loading control). (L) Western blot images showing the effect of YAP
546 overexpression on JIP3 protein abundance in HEK293T cells. HEK 293T cells were transfected
547 either with scramble control or YAP-HA construct. Blots were stained with anti-JIP3, anti-HA (to
548 detect YAP-HA) or or anti-GAPDH (loading control). (M) Wing size quantification of (D-H).

549 **Figure 4. Syd/JIP3 regulates wing size by controlling Diap1 protein turnover**

550 (A-D) Representative images of wing imaginal discs expressing *Syd-RNAi* in the posterior
551 compartment (using *enGAL4* or *HhGAL4*) and stained with antibodies against β-gal to detect Diap1
552 gene activity from a genomic reporter construct, *Diap1-LacZ* (A, B) or antibodies against Diap1 to
553 detect Diap1 protein (C, D). (E-H) Representative images of wing imaginal discs expressing *Syd-*
554 *RNAi* in the posterior compartment in a $diap1^{(33\text{-}1s)}$ heterozygote background and stained with anti-
555 Diap1 antibodies (E, F). Representative images of wing imaginal discs expressing *Syd-RNAi* and
556 stained with TUNEL to detect apoptotic cells are shown in (G, H). Blue color represents DAPI stain
557 to mark DNA. A lateral view image section is shown below (H). Green dotted lines denote anterior
558 (A) and posterior (P) compartment boundaries. (I-P) Representative images showing adult wings
559 from female animals of the indicated genotypes. Control wing images are shown in (I) *nubGAL4*
560 alone, (J) $diap1^{(33\text{-}1s)}$ heterozygotes, and (K) $dronc^{51}$ heterozygotes. Wings derived from *nubGal4*
561 animals expressing *Syd-RNAi* in a wild-type background or under $diap1^{(33\text{-}1s)}$ or $dronc^{51}$
562 heterozygosity are shown in L, M, and N. The respective pseudo-color overlay images are shown in
563 (O, P). Brown images are from (*nubGAL4, Syd-RNAi*) animals. Indigo images are from (*nubGAL4,*
564 *Syd-RNAi*) animals heterozygote either for $diap1^{(33\text{-}1s)}$ (O) or $dronc^{51}$ (P). (Q) Quantification of (I-P)

565 (R) Western blot images showing Diap1 protein levels in dissected third-instar wing discs expressing
566 *srcRFP* alone (control) or co-expressing *Syd-RNAi* in the posterior compartment using *HhGAL4*.
567 Blots were stained with anti-Diap1 or actin (loading control) antibodies. (S) Western blot images
568 showing the effect of JIP3 knockdown on c-IAP protein levels in HEK-293T cells. Lysates were
569 prepared from HEK-293 cells transfected either with scramble control or JIP3-siRNA. Blots were
570 stained with anti-JIP3 antibodies to confirm Jip3 knockdown or anti-c-IAP, or GAPDH (loading
571 control). (T) Graph showing the effect of JIP3 knockdown on HEK-293 cell numbers. (U) Graph
572 showing the comparative proportion of propidium iodide (PI)-positive cells with or without JIP3
573 knockdown using flow cytometry.

574 **Supplemental Figure 1. Syd/JIP3 knockdown in the posterior compartment suppresses adult**
575 **wing size**

576 (A-F) Representative images showing adult wings from female animals of the indicated genotypes
577 (A-E). Syd knockdown effect on wing size using *Syd-RNAi* (*b43232*) (A, B, D, F) or *Syd-RNAi*
578 (*v35346*) (A, C, E, F). (F) Quantification of (A-E).

579 **Supplemental Figure 2. Expression and subcellular localization of ajuba and Warts in Syd**
580 **knockdown cells**

581 (A-C) Lateral section images showing wing imaginal discs containing a genomic rescue construct
582 expressing Ajuba tagged with GFP under its own promoter (*Jub-GFP) (Sabino et al., 2011)* and co-
583 expressing *Syd-RNAi* and RFP (shown in blue) under *ptcGAL4.* Tissues were stained with anti-
584 phosphorylated Warts (pWts) antibodies.

585 **Supplemental Figure 3. *Syd/JIP3* knockdown suppresses *Yorkie*-mediated tissue overgrowth**

586 (A-D) Confocal images of wing imaginal discs from age-controlled animals expression *RFP* (A)
587 alone or co-expressing *Yorkie* (B) or co-expressing *Yorkie* and *Syd-RNAi* (C) under the control of
588 posterior driver *HhGAL4*. (D) Volume quantification of *RFP*-positive tissues in (A-C). Yorkie
589 overexpression caused overgrowth in the posterior compartment and showed an increased RFP-
590 positive area, RFP intensity and tissue folding. Syd depletion (*HhGAL4,Yorkie, Syd-RNAi*) reduced
591 the size of RFP-positive tissues. (E-I) Images of wing imaginal discs from age-controlled animals
592 expressing *RFP* alone (E) or co-expressing *Yorkie* (F and G) or co-expressing *Yorkie* and *Syd-RNAi*
593 (H) under the control of *nubGAL4*. (I) Quantification of (E-H). *Yorkie* overexpression results in
594 overgrown tissues showing severe or moderate tissue folds, 37% and 63% (N=16), respectively.
595 Syd knockdown (*nubGAL4, Yorkie, Syd-RNAi*) suppressed the appearance of tissue folds and
596 yielded tissues with moderate to smooth folding (*N*=16, 56% and 44%, respectively). Severe tissue
597 folding was not detected in (*nubGAL4, Yorkie, Syd-RNAi*) tissues (H).

598 **Supplemental Figure 4. Transcription of *four-jointed* and *cyclin-E* in Syd knockdown cells**

599 (A-I) Representative images of wing imaginal discs dissected from *four-jointed-LacZ* or *CyclinE-*
600 *LacZ* or *Expanded-LacZ* reporter lines expressing *Syd-RNAi* in the posterior compartment using
601 *enGAL4* and stained with antibodies against β-gal to monitor gene activity of *cyclinE* (A-C) or *four-*
602 *jointed* (D-F) or *expanded* (G-I). The insets show that *cyclinE* (B, C) is localized in nucleus while
603 *four-jointed* (E, F) and *expanded* (H, I) are localized at membranes.

604 **Supplemental Figure 5. Mitotic potential of Syd depleted cells**

605 (A, B) Image showing a wing imaginal disc expressing *Syd-RNAi* under the *HhGAL4* driver and
606 stained with anti-phosphorylated Histone-3 to detect proliferating cells. (C) Quantitation of (A, B).
607 *P*-value (t-test) was 0.78.

608 **Supplemental Figure 6. Effect of Diap1 knockdown on adult wing size**

609 (A, B) Images showing wing imaginal discs dissected from female animals of the indicated
610 genotypes. (C) Quantification of (A, B).

611

612 **Supplemental Figure 7. *Syd* gene expression during wing development**

613

614 Graph showing *Syd/JIP3* expression in wing imaginal discs dissected at the indicated developmental
615 time periods from biological triplicates. *Syd/JIP3* expression was calibrated to *Rp49* expression at
616 each developmental time period. Fold expression changes were established by comparing each time
617 period to the 72-80 hours AEL period. Graph shows mean fold changes in gene expression ± SD.

618

619 **Supplemental Figure 8. Full image of presented Western blots**

620 Boxes denotes the data presented in the indicated figures (underlined red text)

621 (A) Full Western blots related to Figure 1F.

622 Anti-JIP3 Western blots from *nubGAL4* (control) or Syd-knockdown (*nubGAL4, Syd-RNAi*) wing
623 tissue lysates. Anti-GAPDH was used as an input control. In *Drosophila*, anti-human JIP3 antibody
624 detected two bands: a prominent ~147KD band and a much weaker 135KD band in lysates derived
625 from wild-type wing tissues. Both of these bands were considerably reduced in lysates obtained from
626 wing tissues expressing Syd-RNAi. Note that the sparse 135KD JIP3 band was not always detected
627 in lysates with lower protein yield.

628 (B) Related to figure 3J. Uncropped images of anti-Syd/JIP3 Western blotting using controls
629 (*nubGal4*) or Hippo knockdown (*nubGal4, HpoRNAi*) larval wing tissue lysates. β-actin is a
630 loading control.

631 (C) Related to figure 3K. Uncropped anti-Syd/JIP3 Western blot image showing Syd/JIP3 protein

632 levels in control (lane#1, *nub-Gal4*) tissues or tissues expressing *Syd-RNAi* (lanes 2 and 3) or

633 overexpressing Yorkie (*nubGal4,Yorkie*) (lane 4). GAPDH is a loading control.

634 (D) Related to figure 3L. Uncropped Western blot images of showing upregulation of JIP3in

635 HEK293 cells overexpressing YAP (YAP-HA) compared to scramble controls. GAPDH is a

636 loading control.

637 (E) Related to figure 4S. Uncropped Western blot images showing the effect of JIP3 knockdown on

638 c-IAP expression in HEK 293 cells.

Figure 1

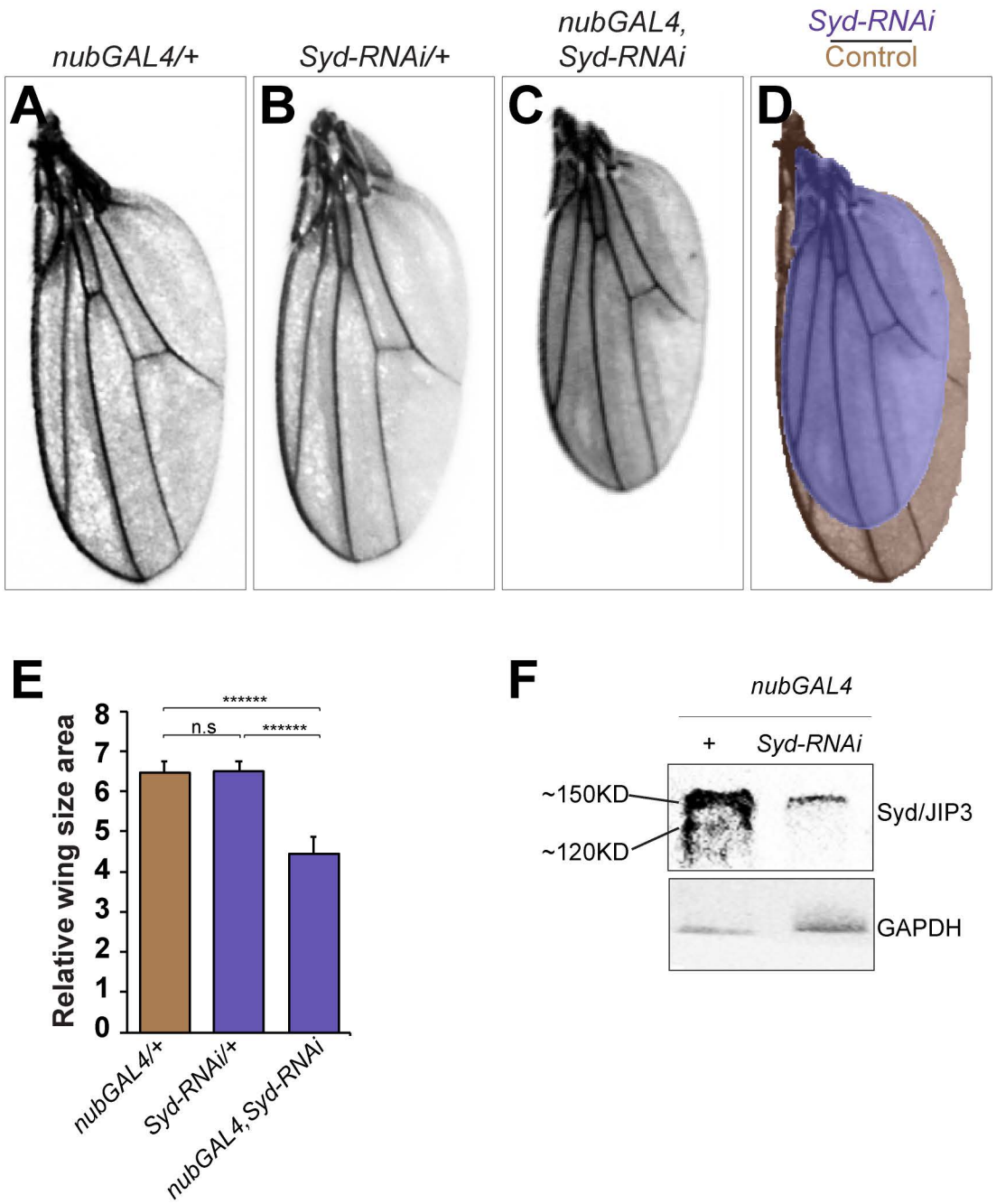
nubGAL4/+
Syd-RNAi/+
nubGAL4, Syd-RNAi
Syd-RNAi
Control
A
B
C
D
E
Relative wing size area
0
1
2
3
4
5
6
7
8
n.s
******
******
nubGAL4/+
Syd-RNAi/+
nubGAL4,Syd-RNAi
F
nubGAL4
+
Syd-RNAi
~150KD
~120KD
Syd/JIP3
GAPDH

Figure 2

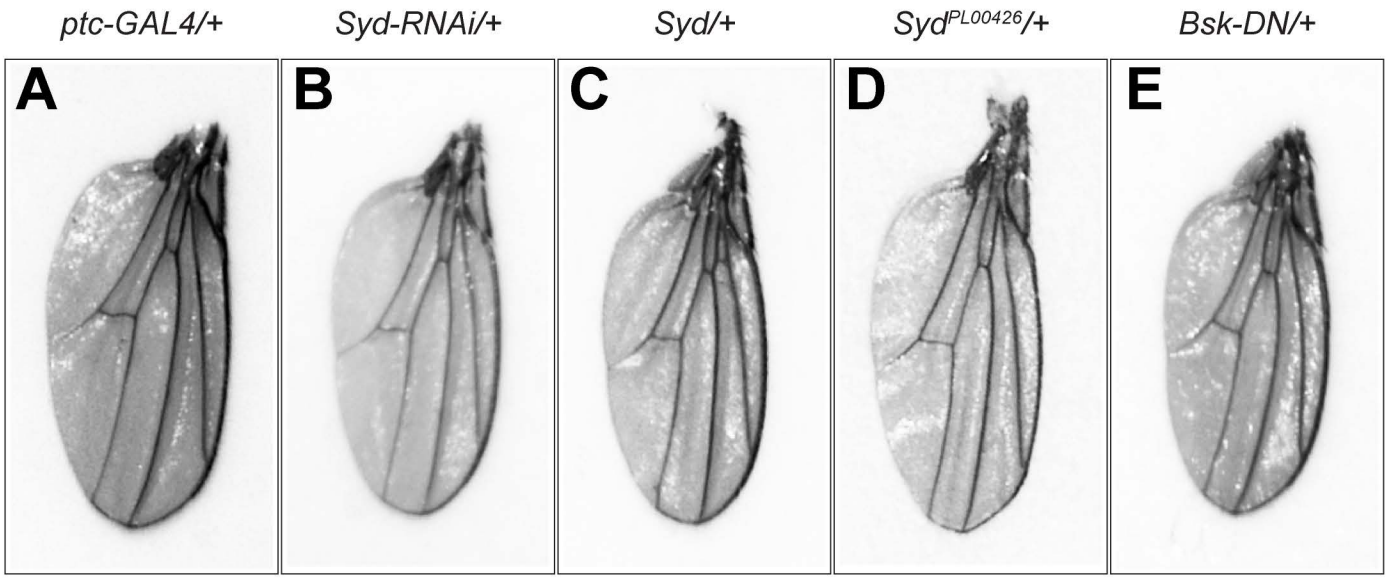
ptc-GAL4/+
Syd-RNAi/+
Syd/+
Syd^PL00426/+
Bsk-DN/+
A
B
C
D
E

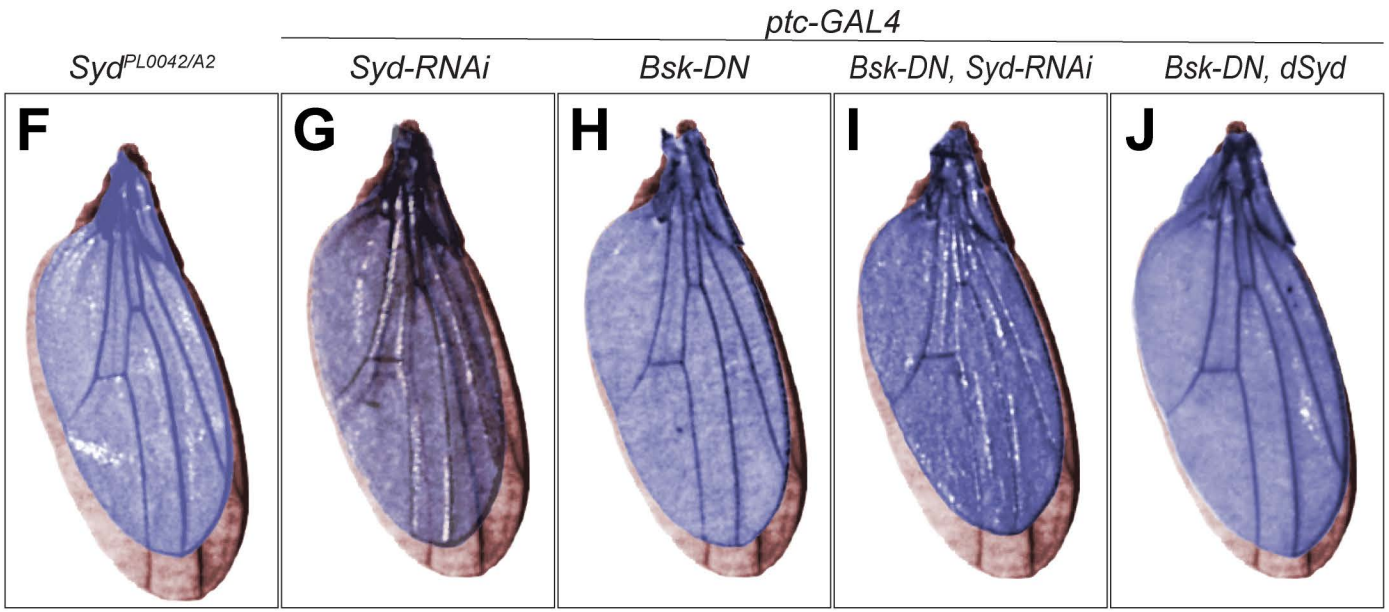
ptc-GAL4
Syd^PL0042/A2
Syd-RNAi
Bsk-DN
Bsk-DN, Syd-RNAi
Bsk-DN, dSyd
F
G
H
I
J

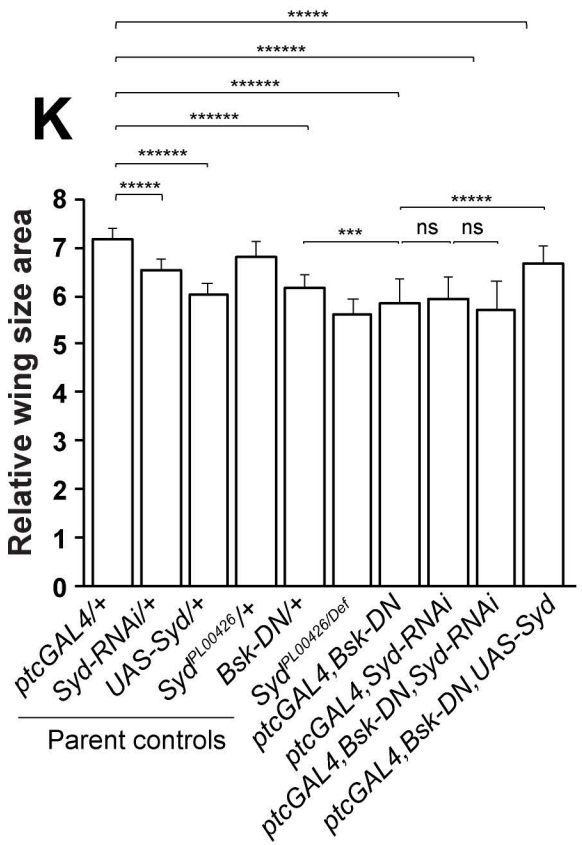
K
Relative wing size area
0
1
2
3
4
5
6
7
8
*****
******
******
******
******
*****
***
ns
ns
*****
ptcGAL4/+
Syd-RNAi/+
UAS-Syd/+
Syd^PL00426/+
Bsk-DN/+
Syd^PL00426/Def
ptcGAL4,Bsk-DN
ptcGAL4,Syd-RNAi
ptcGAL4,Bsk-DN,Syd-RNAi
ptcGAL4,Bsk-DN,UAS-Syd
Parent controls

Figure 3

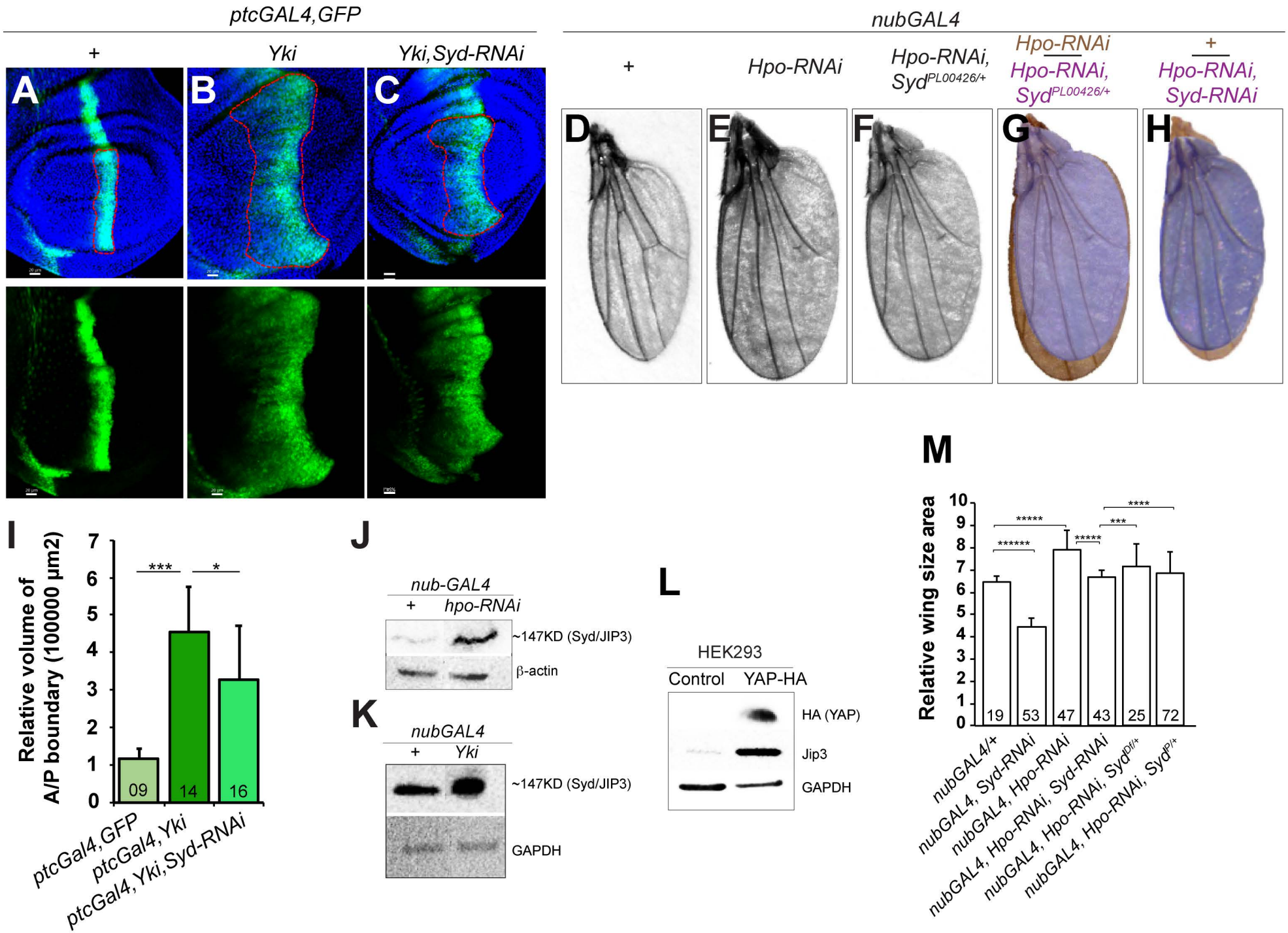
ptcGAL4,GFP
+
Yki
Yki,Syd-RNAi
A
B
C
nubGAL4
+
Hpo-RNAi
Hpo-RNAi, Syd PL00426/+
Hpo-RNAi
Hpo-RNAi, Syd PL00426/+
+
Hpo-RNAi, Syd-RNAi
D
E
F
G
H
I
Relative volume of A/P boundary (100000 µm2)
***
*
09
14
16
ptcGal4,GFP
ptcGal4,Yki
ptcGal4,Yki,Syd-RNAi
J
nub-GAL4
+
hpo-RNAi
~147KD (Syd/JIP3)
β-actin
K
nubGAL4
+
Yki
~147KD (Syd/JIP3)
GAPDH
L
HEK293
Control
YAP-HA
HA (YAP)
Jip3
GAPDH
M
Relative wing size area
19
53
47
43
25
72
nubGAL4/+
nubGAL4, Syd-RNAi
nubGAL4, Hpo-RNAi
nubGAL4, Hpo-RNAi, Syd-RNAi
nubGAL4, Hpo-RNAi, Syd Df/+
nubGAL4, Hpo-RNAi, Syd P/+

Figure 4

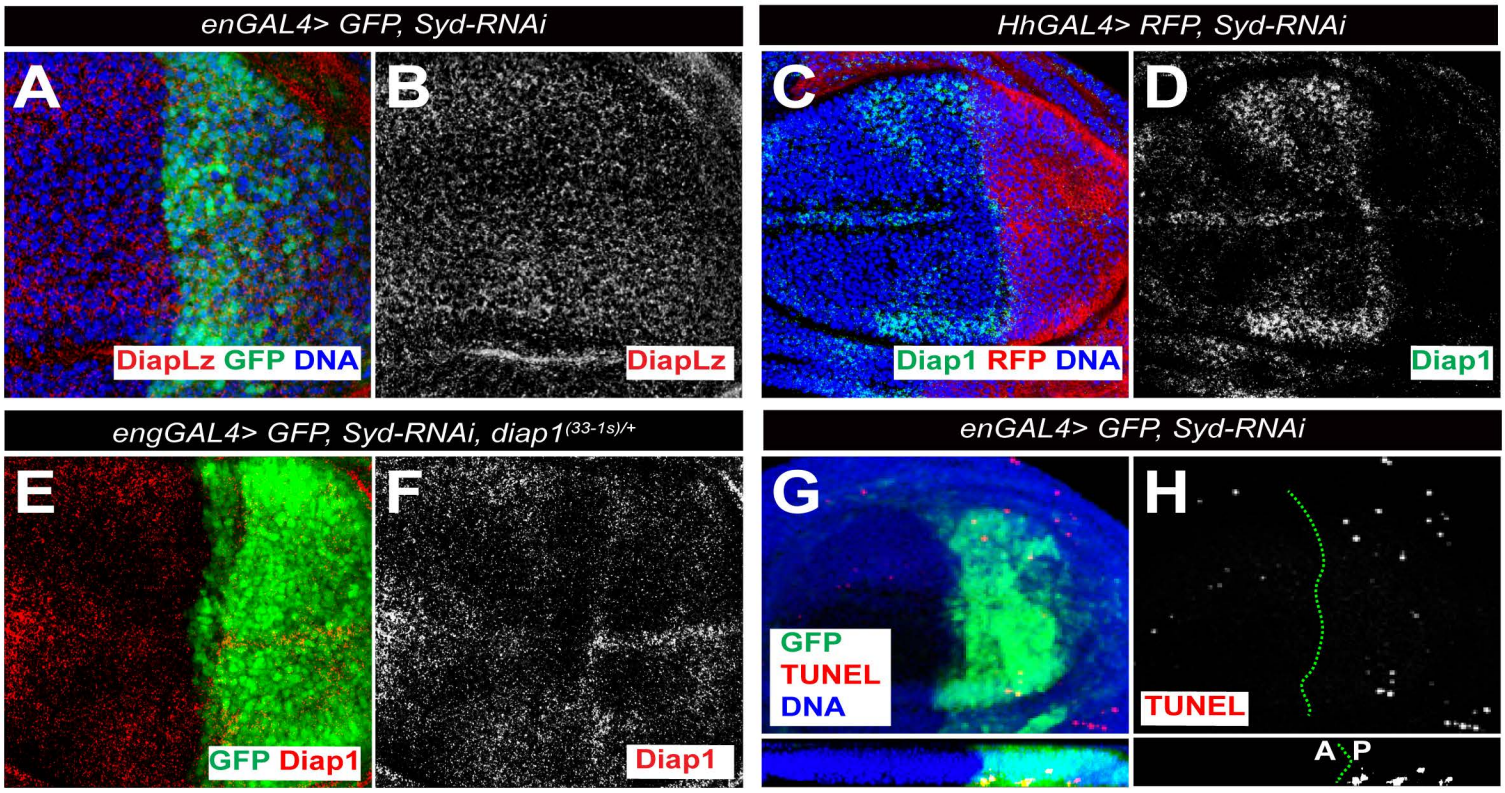
enGAL4> GFP, Syd-RNAi
HhGAL4> RFP, Syd-RNAi
A
B
C
D
DiapLz GFP DNA
DiapLz
Diap1 RFP DNA
Diap1
engGAL4> GFP, Syd-RNAi, diap1(33-1s)/+
enGAL4> GFP, Syd-RNAi
E
F
G
H
GFP Diap1
Diap1
GFP
TUNEL
DNA
TUNEL
A P

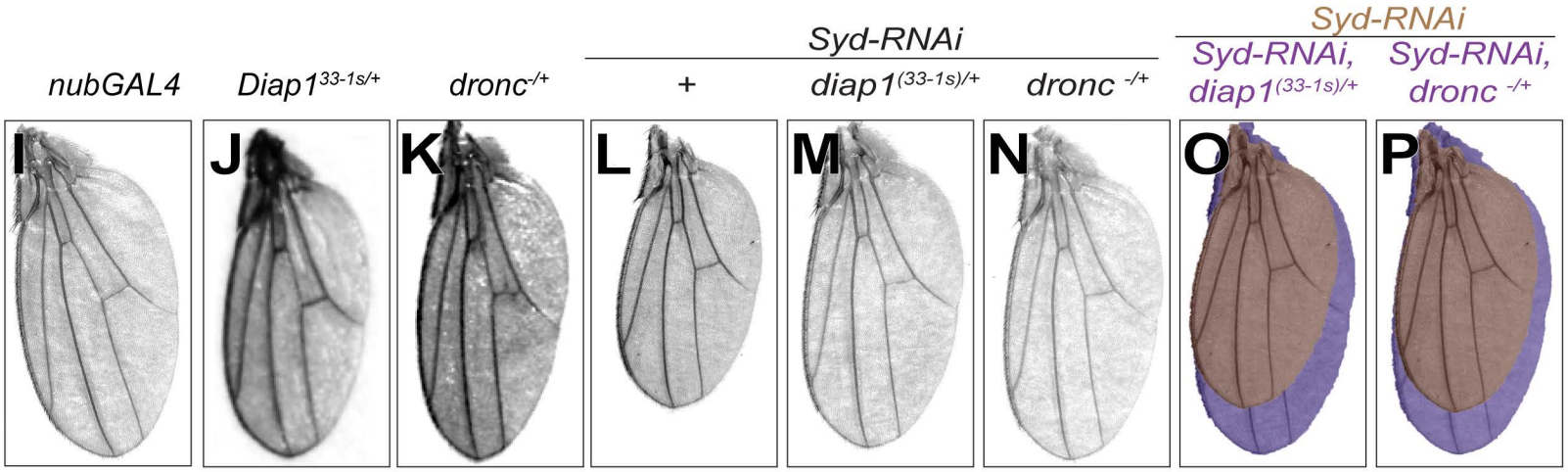
nubGAL4
Diap1 33-1s/+
dronc-/+
Syd-RNAi
+
diap1(33-1s)/+
dronc -/+
Syd-RNAi
Syd-RNAi, diap1(33-1s)/+
Syd-RNAi, dronc -/+
I
J
K
L
M
N
O
P

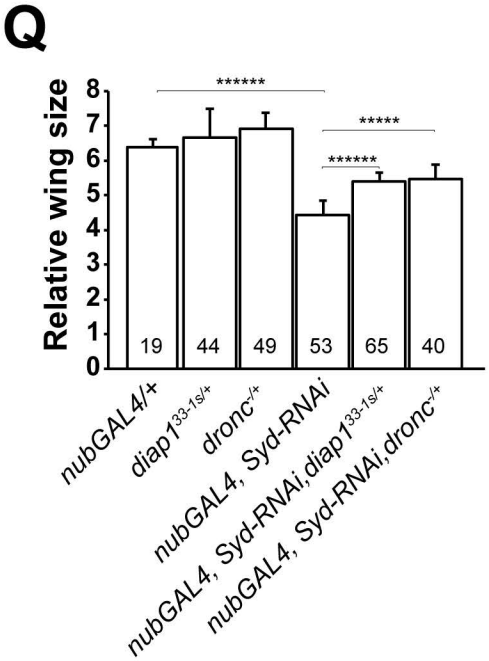
Q
Relative wing size
0
1
2
3
4
5
6
7
8
******
*****
******
19
44
49
53
65
40
nubGAL4/+
diap1 33-1s/+
dronc-/+
nubGAL4, Syd-RNAi
nubGAL4, Syd-RNAi,diap1 33-1s/+
nubGAL4, Syd-RNAi,dronc-/+

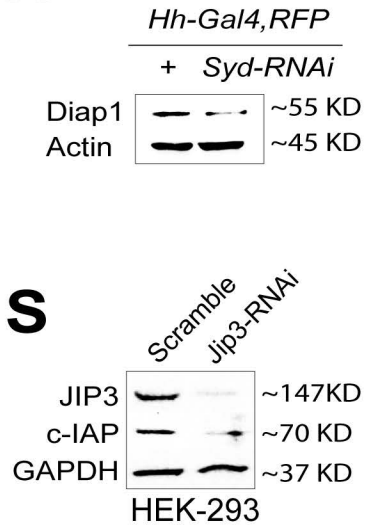
R
Hh-Gal4,RFP
+
Syd-RNAi
Diap1
Actin
~55 KD
~45 KD
S
Scramble
Jip3-RNAi
JIP3
c-IAP
GAPDH
~147KD
~70 KD
~37 KD
HEK-293

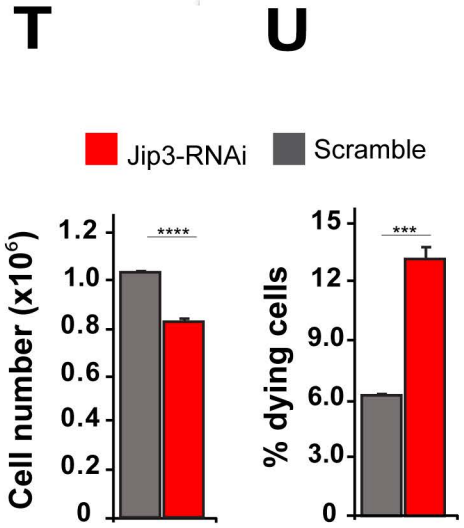
T
U
Jip3-RNAi
Scramble
Cell number (x10^6)
0
0.2
0.4
0.6
0.8
1.0
1.2
****
% dying cells
0
3.0
6.0
9.0
12
15
***

Supplemental Figure 1

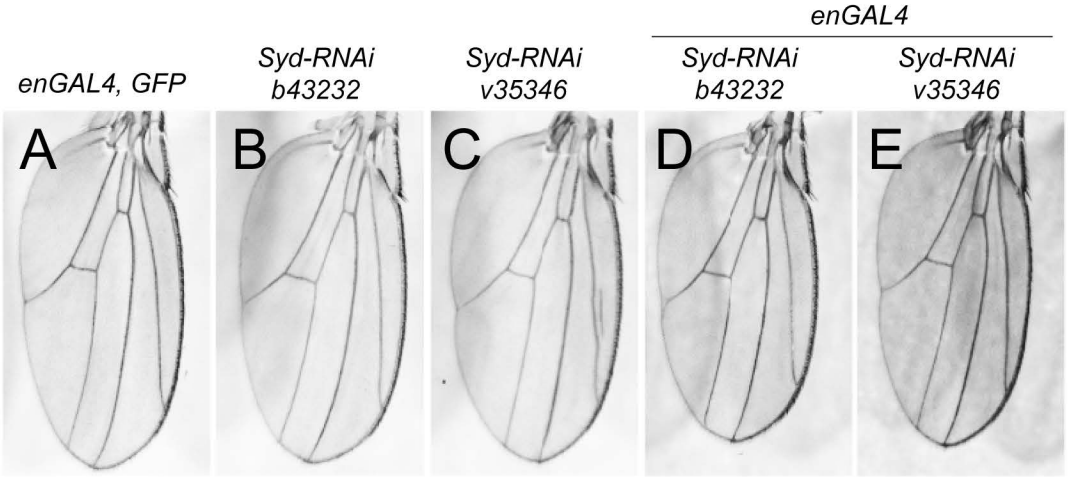

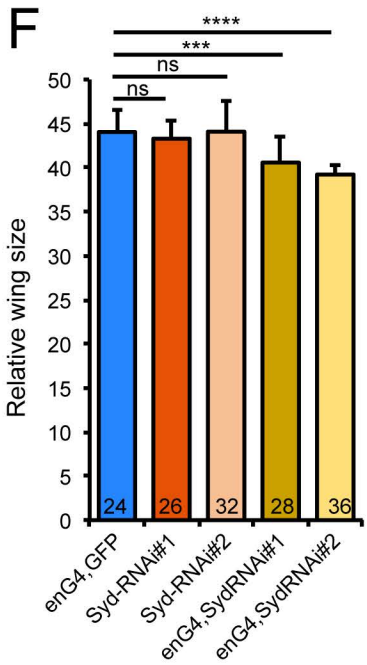

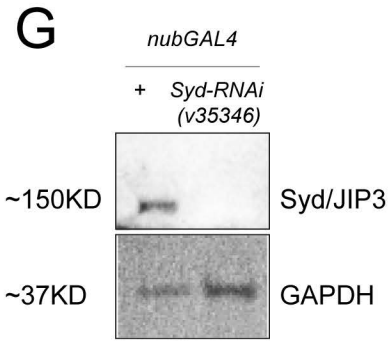

Supplemental Figure 2

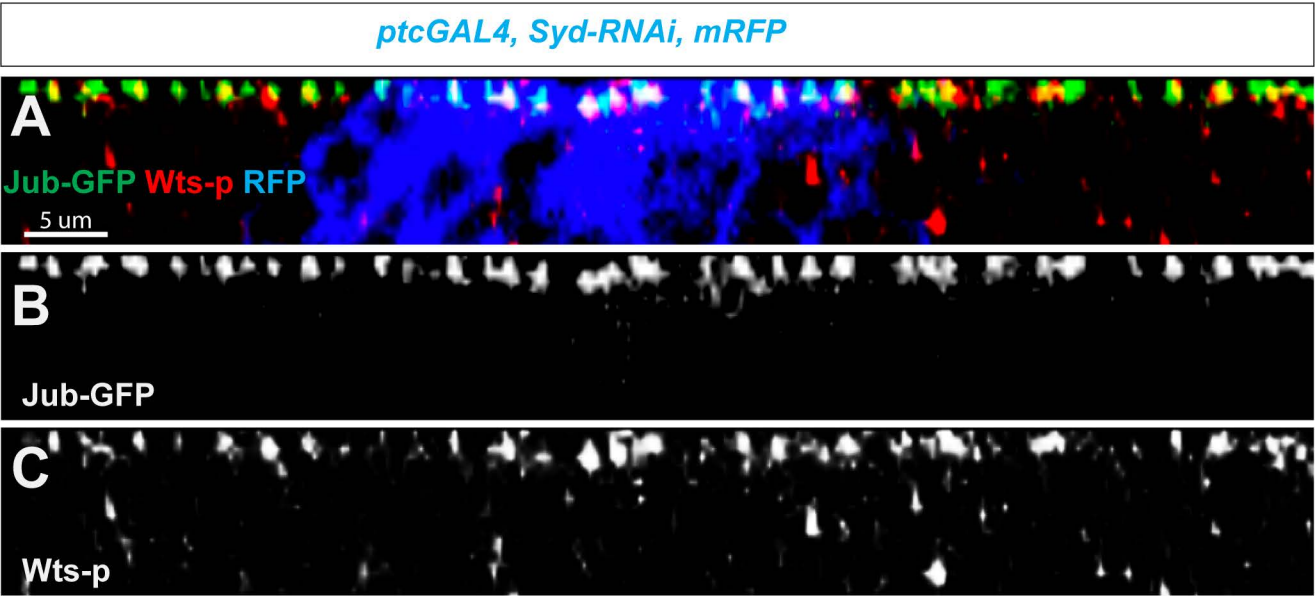

Supplementary Figure 3

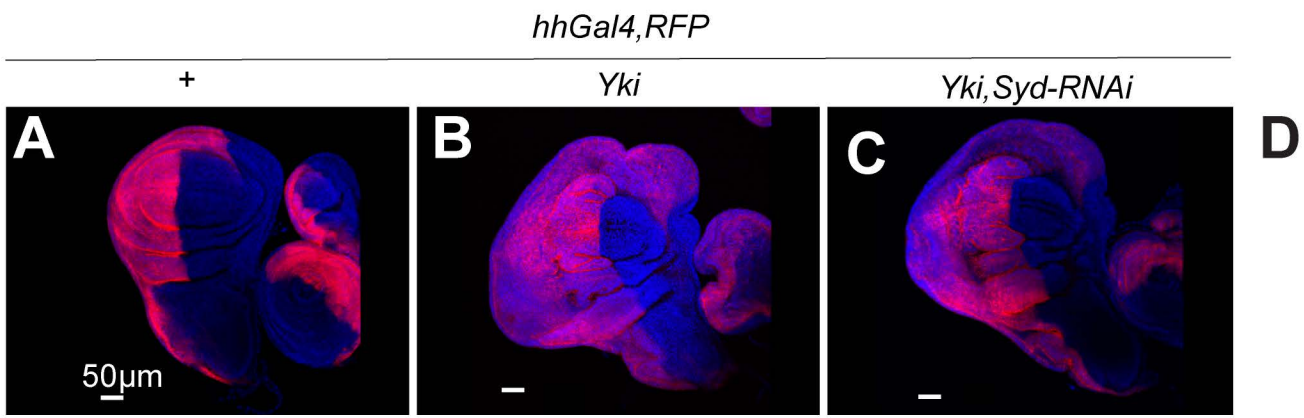

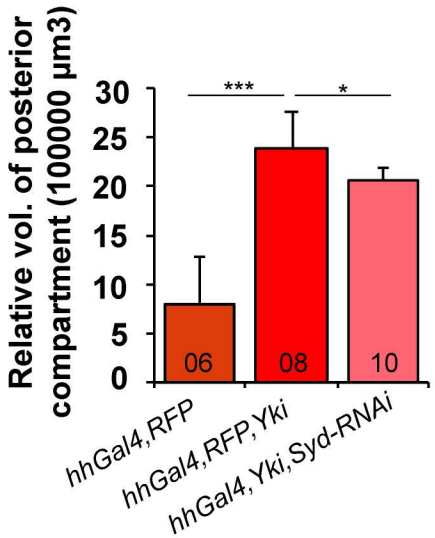

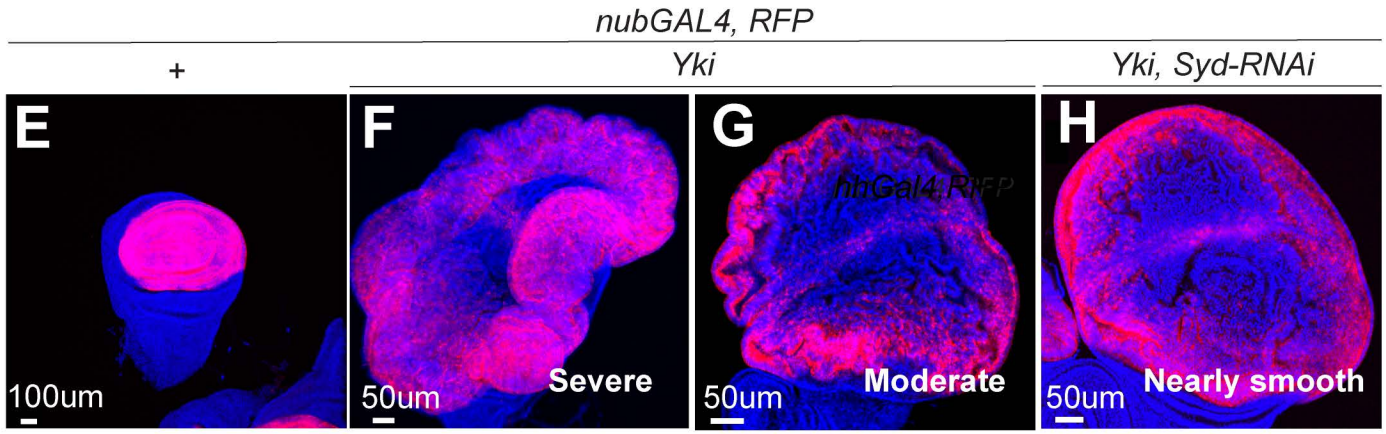

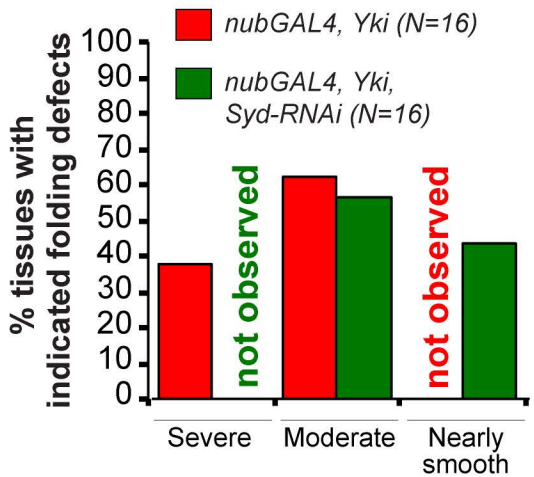

Supplemental Figure 4

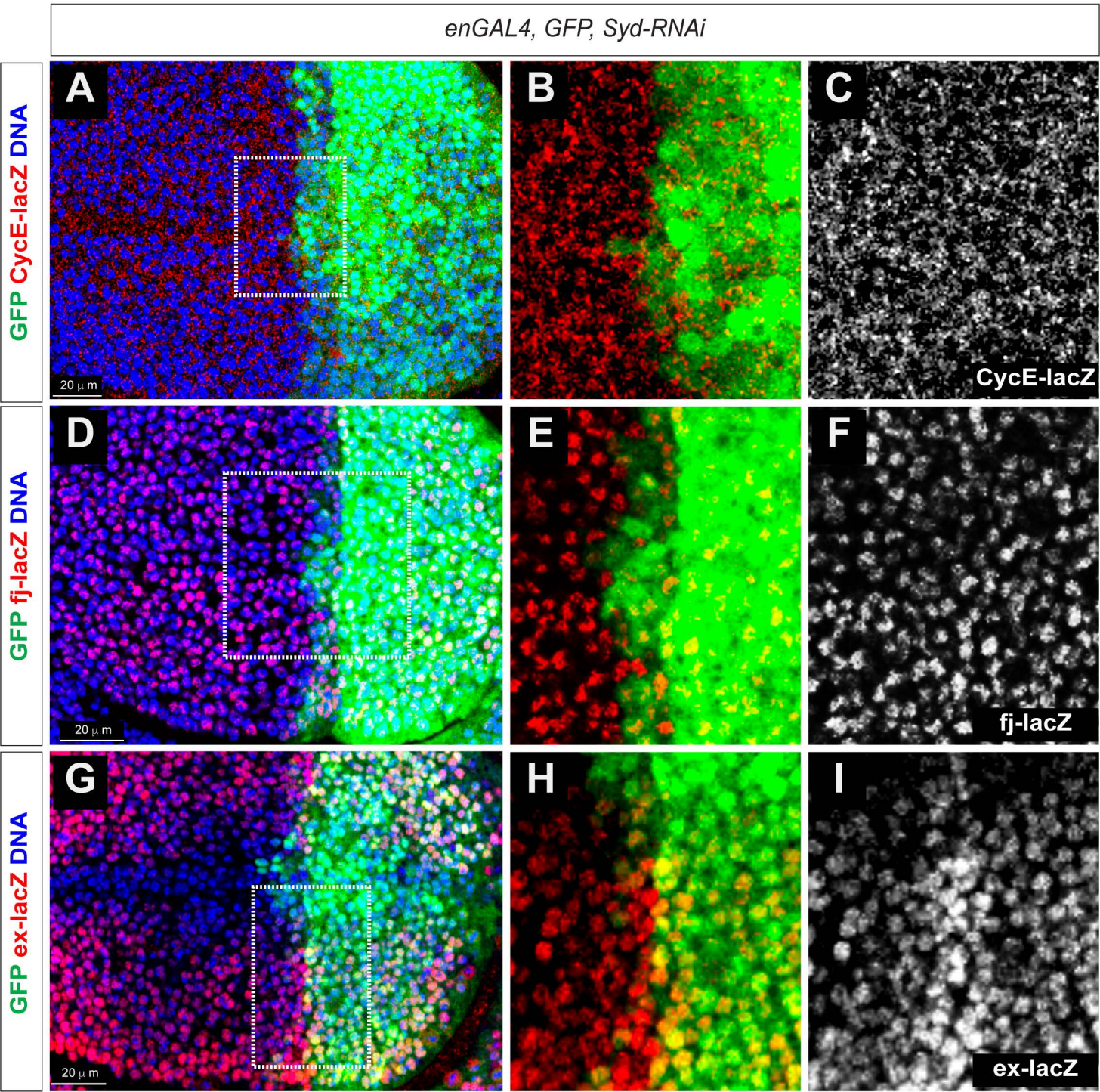

Supplemental Figure 5

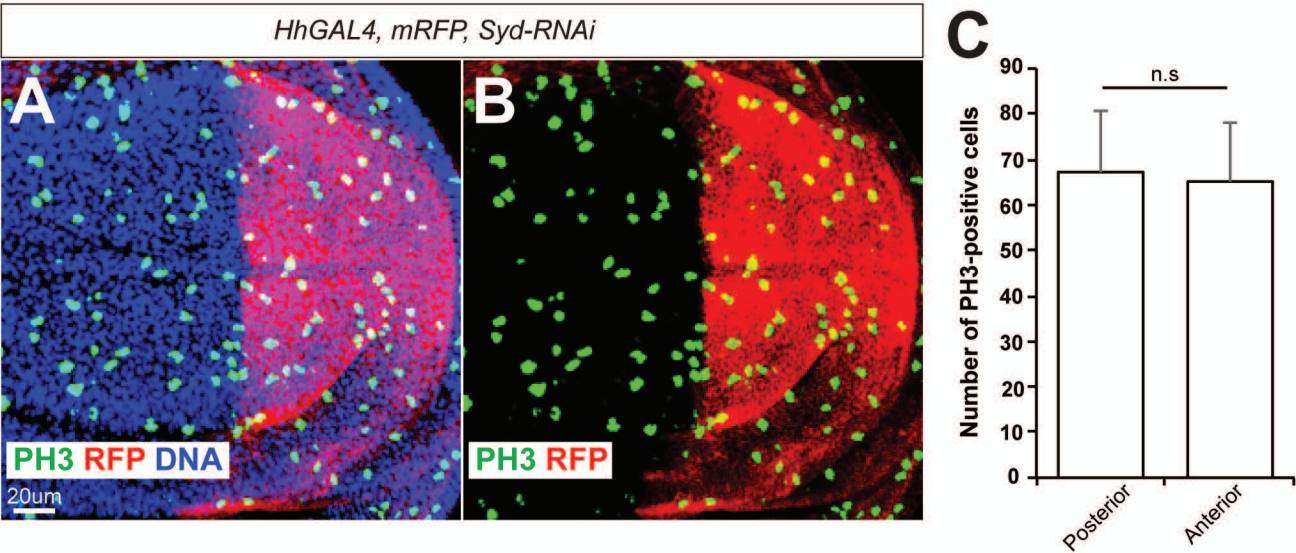

Supplemental Figure 6

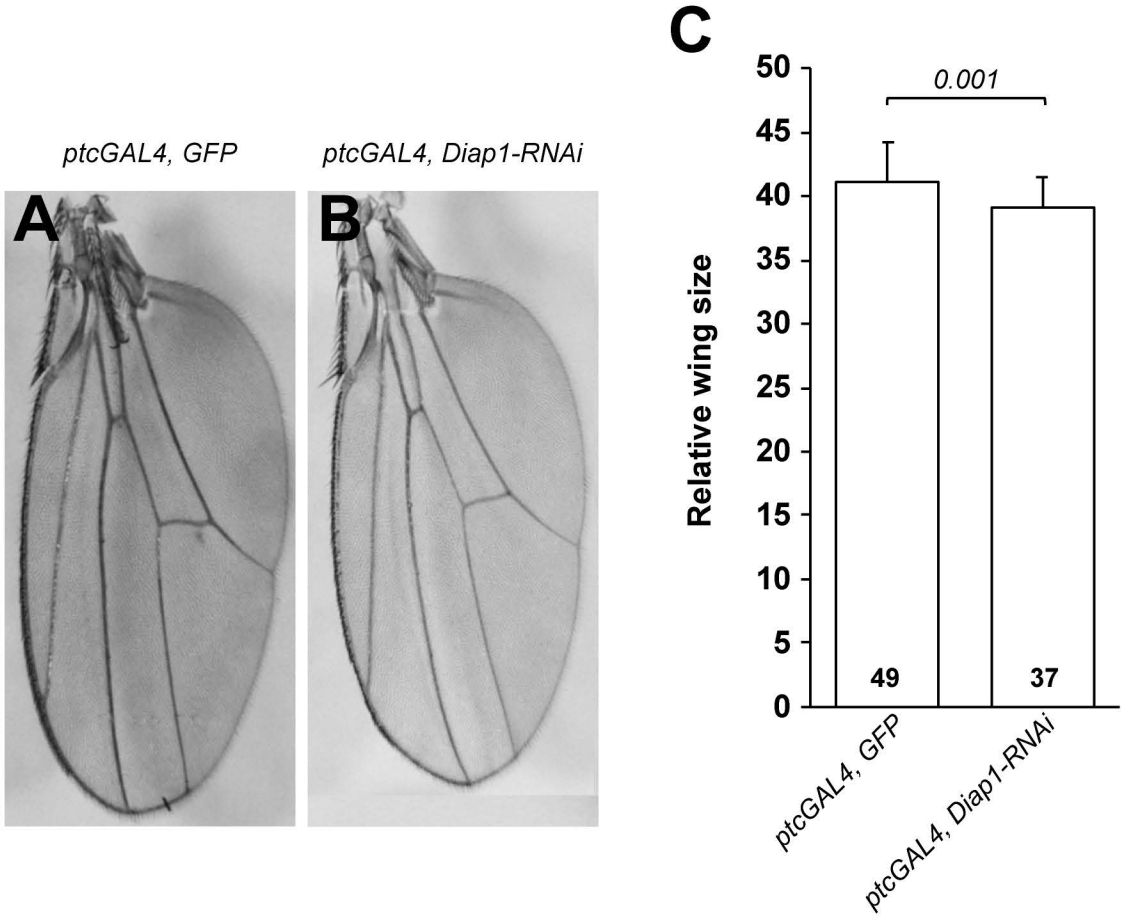

Supplemental Figure 7

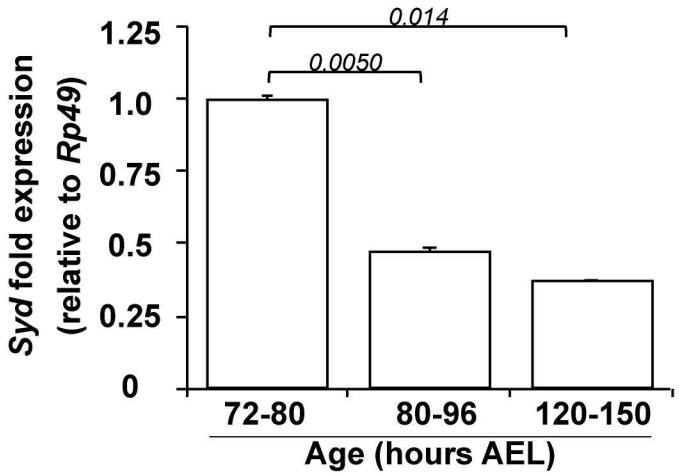
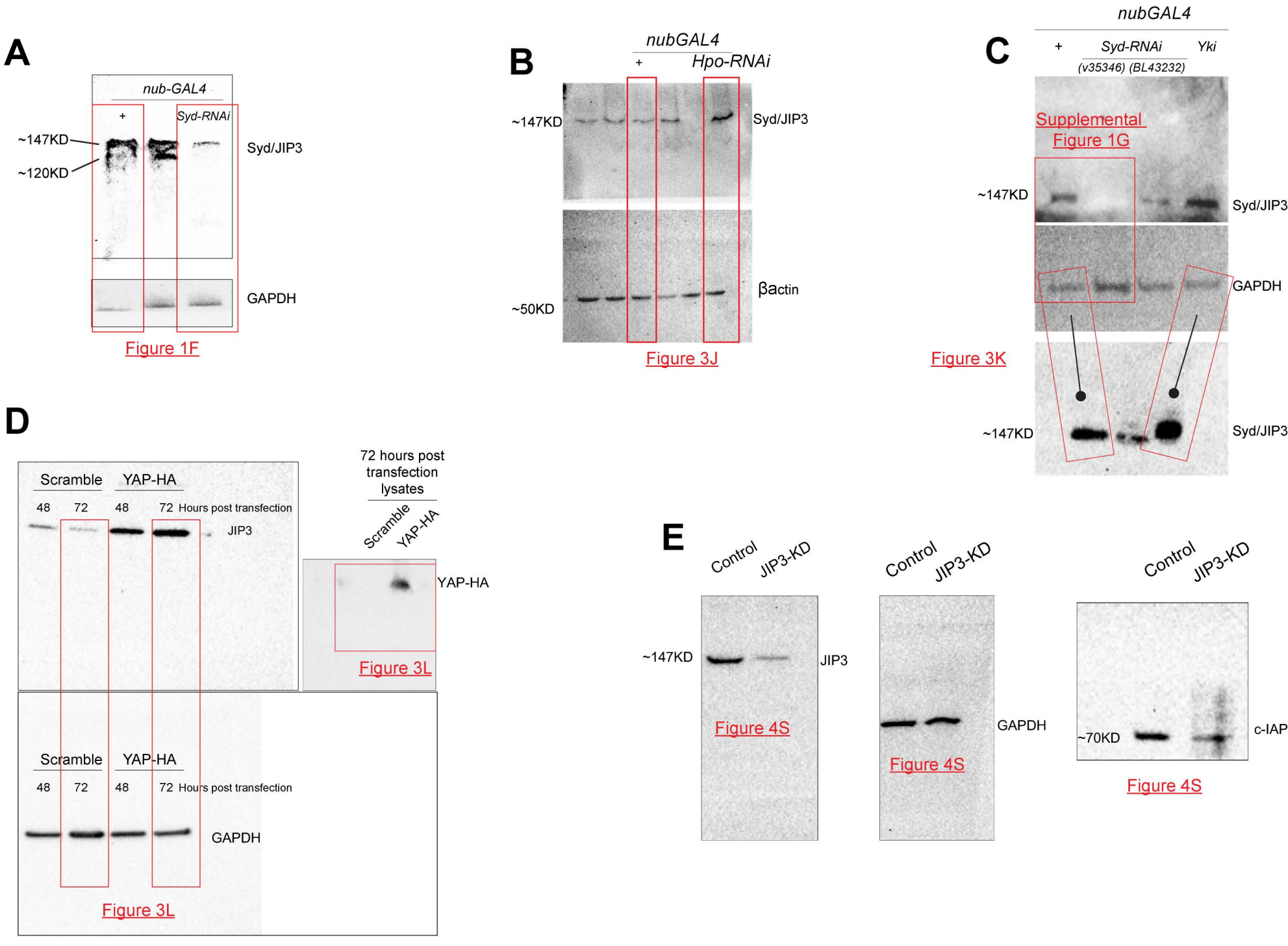
Supplemental Figure 8